CHAPTER 3

Resistance and Propulsion

Chapter Outline

Practical Ship Hydrodynamics. DOI: 10.1016/B978-0-08-097150-6.10003-X

3.1. Resistance and Propulsion Concepts

3.1.1. Interaction Between Ship and Propeller

Any propulsion system interacts with the ship hull. The flow field is changed by the hull. The propulsion system changes, in turn, the flow field at the ship hull. However, traditionally naval architects have considered propeller and ship separately and introduced special efficiencies and factors to account for the effects of interaction. While this decomposition is seen by many as an important aid in structuring the complex problems of ship hydrodynamics, it also hinders a system approach in design and can confuse as much as it can help. Since it is still the backbone of our experimental procedures and ingrained in generations of naval architects, the most important concepts and quantities are covered here. The hope is, however, that in the future CFD will allow a more comprehensive optimization of the ship interacting with the propeller as a whole system.

The general definition 'power = force · speed' yields the effective power

$$P_E = R_T \cdot V_s \tag{3.1}$$

where R_T is the total calm-water resistance of the ship excluding resistance of appendages related to the propulsive organs. Sometimes the rudder is also excluded and treated as part of the propulsion system. (This gives a glimpse of the conceptual confusion likely to follow from different conventions concerning the decomposition. Remember that in the end the installed power is to be minimized. Then 'accounting' conventions for individual factors do not matter. What is lost in one factor will be gained in another.) V_s is the ship speed. P_E is the power we would have to use to tow the ship without a propulsive system.

Following the same general definition of power, we can also define a power formed by the propeller thrust and the speed of advance of the propeller, the so-called thrust power:

$$P_T = T \cdot V_A \tag{3.2}$$

The thrust T measured in a propulsion test is higher than the resistance R_T measured in a resistance test (without propeller). So the propeller induces an additional resistance:

1. The propeller increases the flow velocities in the aftbody of the ship which increases frictional resistance.
2. The propeller decreases the pressure in the aftbody, thus increasing the inviscid resistance.

The second mechanism dominates for usual propeller arrangements. The thrust deduction fraction t couples thrust and resistance:

$$t = 1 - \frac{R_T}{T} \quad \text{or} \quad T(1-t) = R_T \tag{3.3}$$

where t is usually assumed to be the same for model and ship, although the friction component introduces a certain scale effect. Empirical formulae for t are plagued by large margins of uncertainty.

The propeller inflow, i.e. the speed of advance of the propeller V_A, is generally slower than the ship speed due to the ship's wake. The wake is usually decomposed into three components:

- *Friction wake.* Due to viscosity, the flow velocity relative to the ship hull is slowed down in the boundary layer, leading in regions of high curvature (especially in the aftbody) to flow separation.
- *Potential wake.* In an ideal fluid without viscosity and free surface, the flow velocity at the stern resembles the flow velocity at the bow, featuring lower velocities with a stagnation point.
- *Wave wake.* The steady wave system of the ship changes the flow locally as a result of the orbital velocity under the waves. A wave crest above the propeller increases the wake fraction, a wave trough decreases it.

For usual single-screw ships, the frictional wake dominates. Wave wake is only significant for $F_n > 0.3$. The measured wake fraction in model tests is larger than in full scale as boundary layer and flow separation are relatively larger in model scale. Traditionally, correction formulae try to consider this overprediction, but the influence of separation can only be estimated and this introduces a significant error margin. In validation studies, CFD has shown good agreement with model test measurements. It is widely assumed that computing power and turbulence modeling had improved by 2010 to the point where also full-scale computations were expected to be accurate even though they could not be validated explicitly. Despite errors in predicting the wake, the errors in predicting the required power remain small, as the energy loss due to the wake is partially recovered by the propeller. However, the errors in predicting the wake propagate completely when computing optimum propeller rpm and pitch.

The wake behind the ship without propeller is called the nominal wake. The propeller action accelerates the flow field by typically 5−20%. The wake behind the ship with operating propeller is called the effective wake. The wake distribution is either measured by laser-Doppler velocimetry or computed by CFD. CFD also predicts the integral of the wake over the propeller plane, the wake fraction w, well. The wake fraction is defined as:

$$w = 1 - \frac{V_A}{V_s} \tag{3.4}$$

Empirical formulae to estimate w in simple design approaches consider only a few main parameters, but actually the shape of the ship influences the wake considerably. Other important parameters like propeller diameter and propeller clearance are also not explicitly represented in these simple design formulae.

The ratio of the effective power to the thrust power is called the hull efficiency:

$$\eta_H = \frac{P_E}{P_T} = \frac{R_T \cdot V_s}{T \cdot V_A} = \frac{1-t}{1-w} \tag{3.5}$$

So the hull efficiency can be expressed solely by thrust deduction factor t and wake fraction w. η_H can be less or greater than 1. It is thus not really an efficiency, which by definition cannot be greater than 100%.

The power delivered at the propeller can be expressed by the torque and the rpm:

$$P_D = 2\pi \cdot n \cdot Q \tag{3.6}$$

This power is less than the 'brake power' directly at the ship engine P_B due to losses in shaft and bearings. These losses are comprehensively expressed in the shafting efficiency η_S: $P_D = \eta_S \cdot P_B$. The ship hydrodynamicist is not concerned with P_B and can consider P_D as the input power in all further considerations of optimizing the ship hydrodynamics. We use here a simplified definition for the shafting efficiency. Usually marine engineers decompose η_S into a shafting efficiency that accounts for the losses in the shafting only and an additional mechanical efficiency. For the ship hydrodynamicist it suffices to know that the power losses between engine and delivered power are typically 1.5−2%.

The losses from delivered power P_D to thrust power P_T are expressed in the (propeller) efficiency behind ship η_B: $P_T = \eta_B \cdot P_D$.

The open-water characteristics of the propeller are relatively easy to measure and compute. The open-water efficiency η_0 of the propeller is, however, different to η_B. Theoretically, the relative rotative efficiency η_R accounts for the differences between the open-water test and the inhomogeneous three-dimensional propeller inflow encountered in propulsion conditions: $\eta_B = \eta_R \cdot \eta_{B0}$. In reality, the propeller efficiency behind the ship cannot be measured and all effects not included in the hull efficiency, i.e. wake and thrust deduction fraction, are included in η_R. η_R again is not truly an efficiency. Typical values for single-screw ships range from 1.02 to 1.06.

The various powers and efficiencies can be expressed as follows:

$$P_B > P_D > P_T > P_E \tag{3.7}$$

$$P_E = \eta_H \cdot P_T = \eta_H \cdot \eta_B \cdot P_D = \eta_H \cdot \eta_0 \cdot \eta_R \cdot P_D = \eta_H \cdot \eta_0 \cdot \eta_R \cdot \eta_S \cdot P_B = \eta_D \cdot \eta_S \cdot P_B \tag{3.8}$$

The propulsive efficiency η_D collectively expresses the hydrodynamic efficiencies: $\eta_H \cdot \eta_0 \cdot \eta_R$.

3.1.2. Decomposition of Resistance

As the resistance of a full-scale ship cannot be measured directly, our knowledge about the resistance of ships comes from model tests. The measured calm-water resistance is usually

decomposed into various components, although all these components interact and most of them cannot be measured individually. The concept of resistance decomposition is thought to help in designing the hull form as the designer can focus on how to influence individual resistance components. Larsson and Baba (1996) give a comprehensive overview of modern methods of resistance decomposition (Fig. 3.1).

The total calm-water resistance of a new ship hull can be decomposed into:

- *Friction resistance.* Due to viscosity, directly at the ship hull water particles 'cling' to the surface and move with ship speed. A short distance away from the ship, the water particles already have the velocity of an outer, quasi-inviscid flow. The region between the ship surface and the outer flow forms the boundary layer. In the aftbody of a container ship with $R_n \approx 10^9$, the boundary layer thickness may be 1 m. The rapid velocity changes in the normal direction in the boundary layer induce high shear stresses. The integral of the shear stresses over the wetted surface yields the friction resistance.
- *Viscous pressure resistance.* A deeply submerged model of a ship will have no wave resistance, but its resistance will be higher than just the frictional resistance. The form of the ship induces a local flow field with velocities that are sometimes higher and sometimes lower than the average velocity. The average of the resulting shear stresses is then higher. Also, energy losses in the boundary layer, vortices and flow separation prevent an increase to stagnation pressure in the aftbody as predicted in ideal fluid theory. Full ship forms have a higher viscous pressure resistance than slender ship forms.

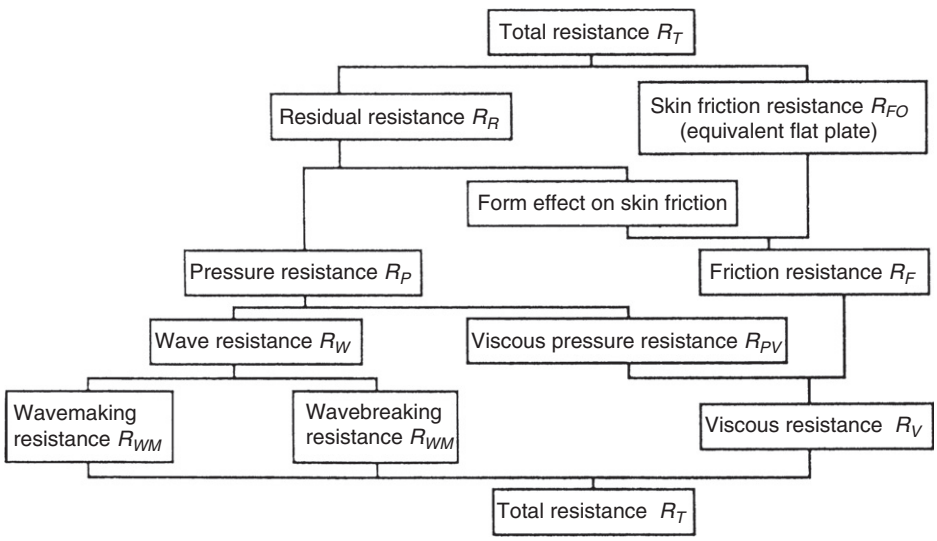

Figure 3.1:
Resistance decomposition

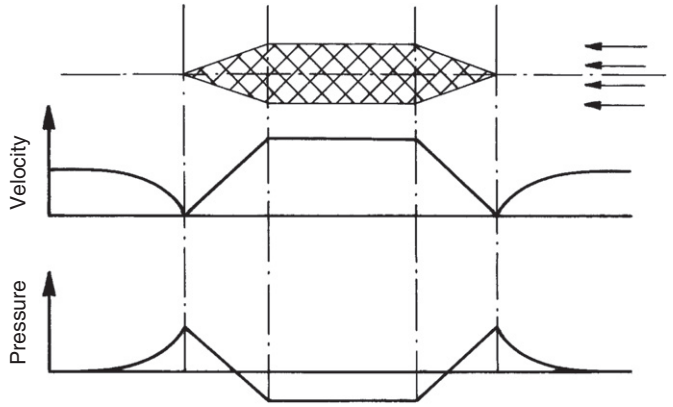

Figure 3.2:
'Primary' wave system

- *Wave resistance.* The ship creates a typical wave system which contributes to the total resistance. In the literature, the wave system is often (rather artificially) decomposed into a primary and a secondary wave system:
  1. Primary wave system (Fig. 3.2)
     In an ideal fluid with no viscosity, a deeply submerged body would have zero resistance (D'Alembert's paradoxon). The flow would be slower at both ends of the body and faster in the middle. Correspondingly at each end, the pressure will be higher than average, reaching at one point stagnation pressure, and the pressure in the middle will be lower than average. Now imagine a body consisting of the ship hull below the calm-water surface and its mirror image at the calm-water surface (Fig. 3.3). This double body would create a certain pressure distribution at the symmetry plane (calm-water surface) in an infinite ideal fluid. Following Bernoulli's equation, we could express a corresponding surface elevation (wave height) distribution for this pressure distribution, yielding wave crests at the ship ends and a long wave trough along the middle. This is called the primary wave system. The shape of the primary wave system is speed independent, e.g. the locations of maxima, minima, and zero crossings are not affected by the speed. The vertical scale (wave height) depends quadratically on the speed.
  2. Secondary wave system (Fig. 3.4)
     At the free surface, a typical wave pattern is produced and radiated downstream. Even if we assume an ideal fluid with no viscosity, this wave pattern will result in a resistance.

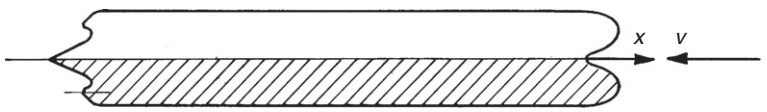

Figure 3.3:
Double-body flow

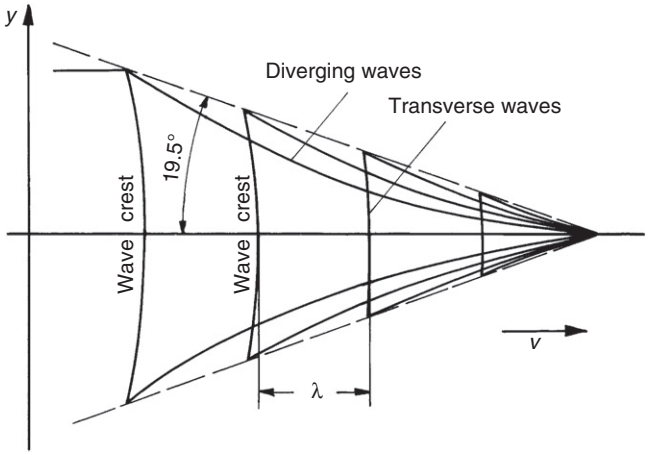

Figure 3.4:
'Secondary' wave system

The wave pattern consists of transverse and divergent waves. In deep water, the wave pattern is limited to a wedge-shaped region with a half-angle of 19.5°. This angle is independent of the actual shape of the ship. On shallow water, the half-angle widens to 90° (for depth Froude number $F_{nh} = 1.0$) and then becomes more and more narrow for supercritical speeds above $F_{nh} = 1$. The ship produces various wave patterns which interfere with each other. The main wave patterns are created where strong changes in the geometry near the water surface occur, i.e. at the bulbous bow, the bow, the forward shoulder, the aft shoulder, and the stern. The wave length λ depends quadratically on the ship speed. Unfavorable Froude numbers with mutual reinforcement between major wave systems, e.g. bow and stern waves, should be avoided. This makes, e.g., $F_n = 0.4$ an unfavorable Froude number. The interference effects result in a wave resistance curve with humps and hollows. If the wave resistance coefficient is considered, i.e. the wave resistance is made non-dimensional by an expression involving the square of the speed, the humps and hollows become very pronounced.

In reality, the problem is more complex:

- The steepness of waves is limited. The pressure in the 'primary wave system' changes rapidly at the ship ends enforcing unrealistically steep waves. In reality, waves break here and change the subsequent 'secondary wave pattern'. At Froude numbers around 0.25 usually considerable wave-breaking starts, making this Froude number often unfavorable, although many textbooks recommend it as favorable based on the above interference argument for the 'secondary wave pattern'.
- The free surface also results in a dynamic trim and sinkage. This also changes the wave pattern. Even if the double-body flow around the dynamically trimmed and sunk ship is computed, this is not really the ship geometry acting on the fluid, as the actually wetted

surface (wave profile) changes the hull. The double-body flow model breaks down completely if a transom stern is submerged, but dry at design speed. This is the case for many modern ship hulls.

The wave resistance cannot be properly estimated by simple design formulae. It is usually determined in model tests. Although efforts to compute the wave resistance by theoretical methods date back more than 100 years, the problem is still not completely solved satisfactorily. The beginning of computational methods is usually seen with the work of the Australian mathematician Michell, who in 1898 proposed an integral expression to compute the wave resistance. Today, boundary element methods have become a standard tool to compute the 'wave resistance problem', but the accurate prediction of the wave resistance only came close to a satisfactory solution by the end of the 1990s. Even then, problems remained with breaking waves and the fundamental dilemma that in reality ship resistance exists only as a whole quantity. Its separation into components is merely a hypothesis to facilitate analysis, but the theoretically cleanly divided resistance components interact and require a comprehensive approach for a completely satisfactory treatment. Free-surface RANSE has made a great deal of progress possible in this respect, despite some remaining problems in capturing accurately breaking waves and spray formation at the ship's bow (Peric and Bertram 2011).

Computational methods for the analysis of the wave resistance will be discussed in detail in Section 3.5.1.

3.2. Experimental Approach

3.2.1. Towing Tanks and Experimental Set-Up

Despite the ever-increasing importance of numerical methods for ship hydrodynamics, model tests in towing tanks are still seen as an essential part in the design of a ship to validate the power requirements in calm water, which form a fundamental part of each contract between shipowner and shipyard.

We owe the modern methodology of predicting a ship's resistance to William Froude, who presented his approach in 1874 to the predecessor of the Royal Institution of Naval Architects in England. His hypothesis was that the ship resistance is divisible into frictional and wavemaking resistance, with the wavemaking resistance following his 'law of comparison' (Froude similarity). This ingenious concept allowed Froude to show, for the first time, how the resistance of a full-scale ship may be determined by testing scale models. His success motivated building the first model basin in 1879 in Torquay, England. Soon further model basins followed in Europe and the USA.

Tests are usually performed in towing tanks, where the water is still and the model is towed by a carriage. (Alternatively, tests can also be performed in circulating tanks, where the model is

still and the water moves.) The carriage in a towing tank keeps its speed with high precision. The model is kept on course by special wires at the ship ends. Usually, models are free to trim and sink. After the initial acceleration, some time has to pass before a stationary state is reached. Then the remaining measuring time is determined by the remaining towing tank distance and the deceleration time of the carriage. Therefore, towing tanks are usually several hundred meters long to allow sufficient measuring time (in most cases).

The model size is determined by a number of boundary conditions:

- The model should be as large as possible to minimize viscous scale effects, especially concerning laminar/turbulent flow and flow separation.
- The model should be small enough to avoid strength problems (both internal strength of the model and loads on the test carriage).
- The model should be small enough such that the corresponding test speed can be achieved by the carriage.
- The model should be small enough to avoid noticeable effects of restricted water in the test basin.

This leads to a bandwidth of acceptable model sizes. Typically models for resistance and propulsion tests have a size $4\,\text{m} \leq L_m \leq 10\,\text{m}$. Model scales range between $15 \leq \lambda \leq 45$. In practice, often the selected stock propeller decides the exact model scale.

Tests are performed keeping Froude similarity, i.e. Froude numbers of model and full scale are the same. The Reynolds numbers differ typically by two orders of magnitude. The scale effect (error of not keeping the Reynolds similarity) is then partially compensated by empirical corrections.

Models operate at considerably lower Reynolds numbers. (Typically for models $R_n \approx 10^7$ and for full-scale ships $R_n \approx 10^9$.) This means that in the model the transition from laminar to turbulent flow occurs relatively further aft. As a consequence, the resistance would be more difficult to scale. Therefore, the model is equipped with artificial turbulence stimulators (sand strip, studs, or trip wire) in the forebody. One assumes that the transition from laminar to turbulent flow occurs at a length corresponding to $R_n = 0.5 \cdot 10^6$ from the stem. In practice, often the turbulence stimulators are located somewhat further aft. Then the reduced resistance due to the longer laminar flow compensates (at least partially) the additional resistance of the turbulence stimulators.

The models are made of special paraffin wax or special tropical wood that hardly changes volume and shape with time or temperature. Wax models are cheaper, but less robust. Wooden models receive a smooth finish of paint. Yellow is the preferred color for regular models as this color contrasts nicely with the (blackish) water, which is important for visual observations, e.g. of the wave profile. For icebreakers, often for similar purposes, red is the preferred color as it appears to be a good compromise for contrasts of water and ice.

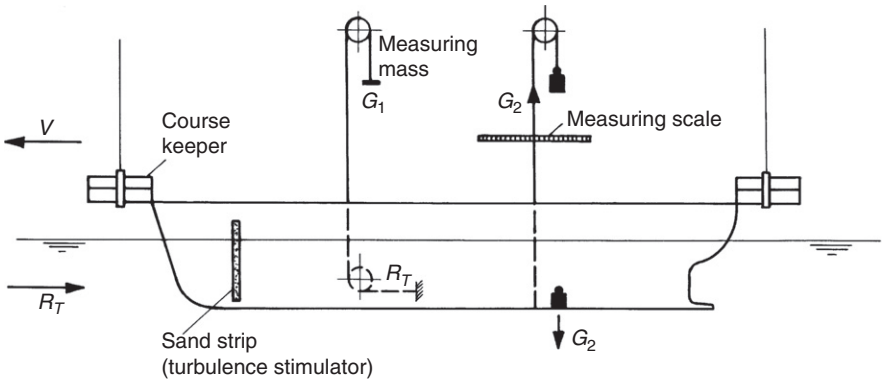

Figure 3.5:
Experimental set-up for resistance test

3.2.2. Resistance Test

Resistance tests determine the resistance of the ship without propeller (and often also without other appendages; sometimes resistance tests are performed for both the 'naked' hull and the hull with appendages). Propulsion tests are performed with an operating propeller and other relevant appendages. A problem is that the forces on appendages are largely driven by viscosity effects with small to negligible gravity effects. As Reynolds similarity is violated, the forces cannot be scaled easily to full scale. For ships with large and unusual appendages, the margins of errors in prediction are thus much larger than for usual hulls, where experience helps in making appropriate corrections.

The model is towed by weights and wires (Fig. 3.5). The main towing force comes from the main weight G_1. The weight G_2 is used for fine-tuning:

$$R_T = G_1 \pm G_2 \sin \alpha \tag{3.9}$$

The sign is positive if the vertical wire moves aft. The angle α is determined indirectly by measuring the distance on the length scale. Alternatively, modern experimental techniques also use strain gauges as these do not tend to oscillate as the wire-weight systems do.

The model test gives the resistance (and power) for towing tank conditions:

- (usually) sufficiently deep water;
- no seaway;
- no wind;
- fresh water at room temperature.

This model resistance has to be converted for a prediction of the full-scale ship. To do this conversion several methods are outlined in the following chapters, namely:

- Method ITTC 1957;
- Method of Hughes–Prohaska;
- Method ITTC 1978;
- Geosim method of Telfer.

The most important of these methods in practice is the method ITTC 1978. Resistance tests are also used to measure the nominal wake, i.e. the wake of the ship without propeller. Measurements of the nominal wake are usually limited to the propeller plane. The local velocities were traditionally measured by pitot tubes. Laser-Doppler velocimetry also allows non-intrusive measurements of the flow field. The results are usually displayed as contour lines of the longitudinal component of the velocity (Fig. 3.6). These data play an important role in the design of a propeller. For optimizing the propeller pitch as a function of the radial distance from the hub, the wake fraction is computed as a function of this radial distance by integrating the wake in the circumferential direction:

$$w(r) = \frac{1}{2\pi} \int_0^{2\pi} w(r, \phi)\, \mathrm{d}\phi \tag{3.10}$$

The wake field is also used in evaluating propeller-induced vibrations.

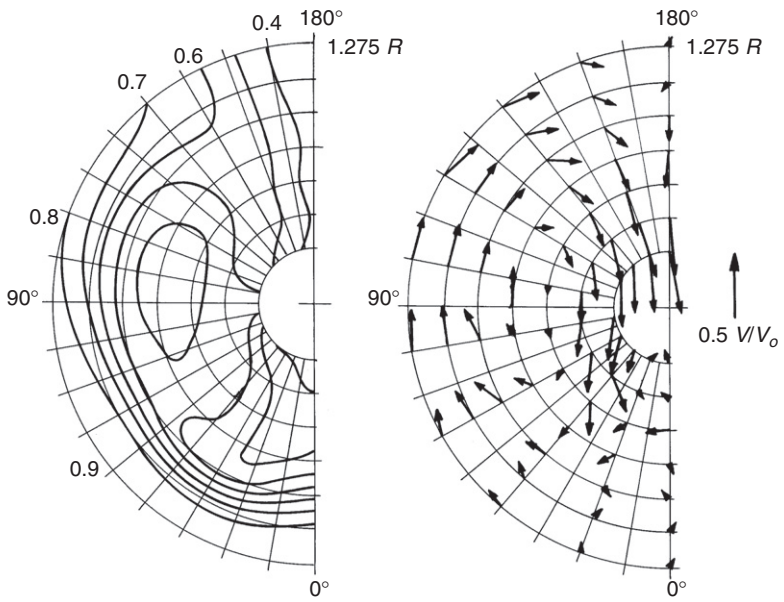

Figure 3.6:
Results of wake measurement

3.2.3. Method ITTC 1957

The resistance of the hull is decomposed as:

$$R_T = R_F + R_R \tag{3.11}$$

R_F is the frictional resistance, R_R the residual resistance. Usually the resistance forces are expressed as non-dimensional coefficients of the form:

$$c_i = \frac{R_i}{\frac{1}{2}\rho V_s^2 S} \tag{3.12}$$

S is the wetted surface in calm water, V_s the ship speed. The resistance coefficient of the ship is then determined as:

$$c_{Ts} = c_{Fs} + c_R + c_A = c_{Fs} + (c_{Tm} - c_{Fm}) + c_A \tag{3.13}$$

The index s again denotes values for the full-scale ship, the index m values for the model. c_R is assumed to be independent of model scale, i.e. c_R is the same for model and full scale. The model test serves primarily to determine c_R. The procedure is as follows:

1. Determine the total resistance coefficient in the model test:

$$c_{Tm} = \frac{R_{Tm}}{\frac{1}{2}\rho_m V_m^2 S_m} \tag{3.14}$$

2. Determine the residual resistance, the same for model and ship:

$$c_R = c_{Tm} - c_{Fm} \tag{3.15}$$

3. Determine the total resistance coefficient for the ship:

$$c_{Ts} = c_R + c_{Fs} + c_A \tag{3.16}$$

4. Determine the total resistance for the ship:

$$R_{Ts} = c_{Ts} \cdot \frac{1}{2}\rho_s V_s^2 S_s \tag{3.17}$$

The frictional coefficients c_F are determined by the ITTC 1957 formula:

$$c_F = \frac{0.075}{(\log_{10} R_n - 2)^2} \tag{3.18}$$

Table 3.1: Recommended values for c_A

L_{pp} (m)	c_A
50–150	0.00035–0.0004
150–210	0.0002
210–260	0.0001
260–300	0
300–350	−0.0001
>350	−0.00025

This formula already contains a global form effect, increasing the value of c_F by 12% compared to the value for flat plates (Hughes formula).

Historically c_A was a roughness allowance coefficient which considered that the model was smooth while the full-scale ship was rough, especially when ship hulls were still riveted. However, with the advent of welded ships c_A sometimes became negative for fast and big ships. Therefore, c_A is more appropriately termed the correlation coefficient. c_A encompasses collectively all corrections, including roughness allowance, but also particularities of the measuring device of the model basin, errors in the model–ship correlation line, and the method. Model basins use c_A not as a constant, but as a function of the ship size, based on experience. The correlation coefficient makes predictions from various model basins difficult to compare and may in fact be abused to derive overly optimistic speed predictions to please customers.

Formulae for c_A differ between various model basins and shipyards. Examples are Table 3.1 and:

$$c_A = 0.35 \cdot 10^{-3} - 2 \cdot L_{pp} \cdot 10^{-6} \tag{3.19}$$

3.2.4. Method of Hughes–Prohaska

This approach decomposes the total resistance (coefficient) as follows:

$$c_T = (1 + k) \cdot c_{F0} + c_w \tag{3.20}$$

Both form factor $(1 + k)$ and wave resistance coefficient c_w are assumed to be the same for model and full scale, i.e. independent of R_n. The model test serves primarily to determine the wave resistance coefficient. The procedure is as follows:

1. Determine the total resistance coefficient in the model test as for the ITTC 1957 method:

$$c_{Tm} = \frac{R_{Tm}}{\frac{1}{2}\rho_m V_m^2 S_m} \tag{3.21}$$

2. Determine the wave resistance coefficient, the same for model and ship:

$$c_w = c_{Tm} - c_{F0m} \cdot (1 + k) \tag{3.22}$$

3. Determine the total resistance coefficient for the ship:

$$c_{Ts} = c_w + c_{F0s} \cdot (1 + k) + c_A \tag{3.23}$$

4. Determine the total resistance for the ship:

$$R_{Ts} = c_{Ts} \cdot \frac{1}{2} \rho_s V_s^2 S_s \tag{3.24}$$

The frictional coefficients c_{F0} for flat plates are determined by Hughes' formula:

$$c_F = \frac{0.067}{(\log_{10} R_n - 2)^2} \tag{3.25}$$

The correlation coefficient c_A differs fundamentally from the correlation coefficient for the ITTC 1957 method. Here c_A does not have to compensate for scaling errors of the viscous pressure resistance. ITTC recommends universally $c_A = 0.0004$.

The Hughes–Prohaska method is a form factor method. The form factor $(1 + k)$ is assumed to be independent of F_n and R_n and the same for model and ship. The form factor is determined by assuming:

$$\frac{c_T}{c_{F0}} = (1 + k) + \alpha \frac{F_n^4}{c_{F0}} \tag{3.26}$$

Model test results for several Froude numbers (e.g. between 0.12 and 0.24) serve to determine α in a regression analysis (Fig. 3.7).

3.2.5. Method of ITTC 1978

This approach is a modification of the Hughes–Prohaska method. It is generally more accurate and also considers the air resistance. The total resistance (coefficient) is again written in a form factor approach:

$$c_{Ts} = (1 + k) c_{Fs} + c_w + c_A + c_{AA} \tag{3.27}$$

c_w is the wave resistance coefficient, assumed to be the same for model and ship, i.e. independent of R_n. c_{Fs} is the frictional coefficient, following the ITTC 1957 formula. c_A is the correlation coefficient, which depends on the hull roughness:

$$c_A \cdot 10^3 = 105 \cdot \sqrt[3]{\frac{k_s}{L_{oss}}} - 0.64 \tag{3.28}$$

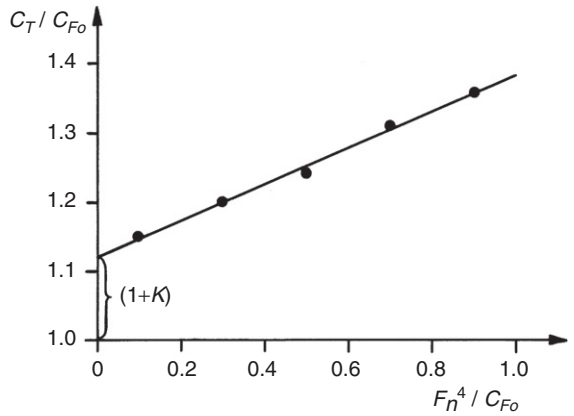

Figure 3.7:
Extrapolation of form factor

where k_s is the roughness of the hull and L_{oss} is the wetted length of the full-scale ship. For new ships, a typical value is $k_s/L_{oss} = 10^{-6}$, i.e. $c_A = 0.00041$.

c_{AA} considers globally the air resistance as follows:

$$c_{AA} = 0.001 \cdot \frac{A_T}{S} \tag{3.29}$$

where A_T is the frontal area of the ship above the waterline and S the wetted surface.

The model test serves primarily to determine the wave resistance coefficient. The procedure is similar to the procedure for Hughes−Prohaska, but the frictional coefficient is determined following the ITTC 1957 formula instead of Hughes' formula. The form factor is also determined slightly differently:

$$\frac{c_T}{c_F} = (1 + k) + \alpha \cdot \frac{F_n^n}{c_F} \tag{3.30}$$

Both n and α are determined in a regression analysis.

3.2.6. Geosim Method of Telfer

Telfer proposed in 1927 to perform model tests with families of models which are *geo*metrically *sim*ilar, but have different model scale. This means that tests are performed at the same Froude number, but different Reynolds numbers. The curve for the total resistance as a function of the Reynolds number is then used to extrapolate to the full-scale Reynolds number.

Telfer plotted the total resistance coefficient over log $R_n^{-1/3}$. For each model, a curve of the resistance is obtained as a function of F_n. Points of the same Froude number for various model scales are connected by a straight line which is easily extrapolated to full scale.

Telfer's method is regarded as the most accurate of the discussed prediction methods and avoids theoretically questionable decomposition of the total resistance. However, it is used only occasionally for research purposes as the costs for the model tests are too high for practical purposes.

3.2.7. Propulsion Test

Propulsion tests are performed to determine the power requirements, but also to supply wake and thrust deduction, and other input data (such as the wake field in the propeller plane) for the propeller design. The ship model is then equipped with a nearly optimum propeller selected from a large stock of propellers, the so-called stock propeller. The actual optimum propeller can only be designed after the propulsion test. The model is equipped with a propulsive drive, typically a small electro-motor (Fig. 3.8).

The tests are again performed for Froude similarity. The total resistance coefficient is then higher than for the full-scale ship, since the frictional resistance coefficient decreases with increasing Reynolds number. This effect is compensated by applying a 'friction deduction' force. This compensating force is determined as follows (see Section 3.2.5):

$$F_D = \frac{1}{2}\rho \cdot V_m^2 \cdot S_m \cdot ((1+k)(c_{Fm} - c_{Fs}) - c_A - c_{AA}) \tag{3.31}$$

The propeller then has to produce a thrust that has to compensate the total resistance R_T minus the compensating force F_D. The propulsion test is conducted with constant speed. The rpm of the propeller is adjusted such that the model is in self-propelled equilibrium. Usually the speed of the towing tank carriage is kept constant and the rpm of the propeller varied until an equilibrium is

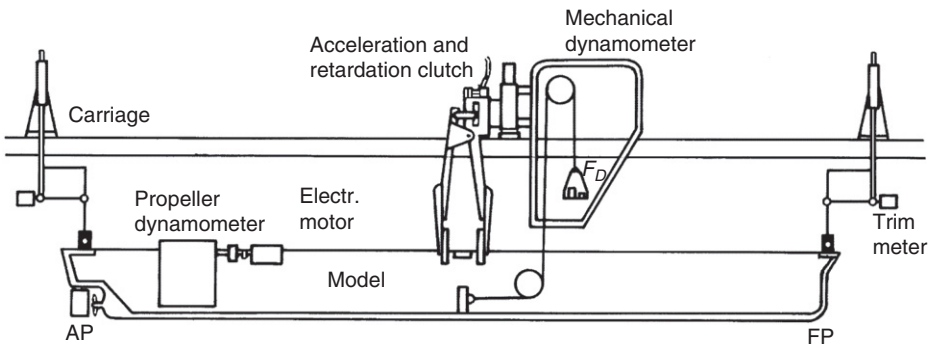

Figure 3.8:
Experimental set-up for propulsion test

reached. A propeller dynamometer then measures thrust and torque of the propeller as a function of speed. In addition, dynamical trim and sinkage of the model are recorded. The measured values can be transformed from model scale to full scale by the similarity laws: speed $V_s = \sqrt{\lambda} \cdot V_m$, rpm $n_s = n_m/\sqrt{\lambda}$, thrust $T_s = T_m \cdot (\rho_s/\rho_m) \cdot \lambda^3$, torque $Q_s = Q_m \cdot (\rho_s/\rho_m) \cdot \lambda^4$. A problem is that the propeller inflow is not geometrically similar for model and full scale due to the different Reynolds number. Thus the wake fraction is also different. Also, the propeller rpm should be corrected to be appropriate for the higher Reynolds number of the full-scale ship.

The scale effects on the wake fraction are attempted to be compensated by the empirical formula:

$$w_s = w_m \cdot \frac{c_{Fs}}{c_{Fm}} + (t + 0.04) \cdot \left(1 - \frac{c_{Fs}}{c_{Fm}}\right) \tag{3.32}$$

t is the thrust deduction coefficient and is assumed to be the same for model and full scale.

The evaluation of the propulsion test requires the resistance characteristics and the open-water characteristics of the stock propeller. There are two approaches:

1. *'Thrust identity' approach*. The propeller produces the same thrust in a wake field of wake fraction w as in open water with speed $V_s(1 - \mathrm{w})$ for the same rpm, fluid properties, etc.
2. *'Torque identity' approach*. The propeller produces the same torque in a wake field of wake fraction w as in open water with speed $V_s(1 - \mathrm{w})$ for the same rpm, fluid properties, etc.

The ITTC standard is the 'thrust identity' approach. It will be covered in more detail in the next chapter on the ITTC 1978 performance prediction method.

The results of propulsion tests are usually given in diagrams, as shown in Fig. 3.9. Delivered power and propeller rpm are plotted over speed. The results of the propulsion test prediction are validated in the sea trial of the ship introducing necessary corrections for wind, seaway, and shallow water. The diagrams contain not only the full-load design condition at trial speed, but also ballast conditions and service speed conditions. Service conditions feature higher resistance, reflecting the reality of the ship after some years of service: increased hull roughness due to fouling and corrosion, added resistance in seaway and wind.

3.2.8. ITTC 1978 Performance Prediction Method

The ITTC 1978 performance prediction method (IPPM78) has become a widely accepted procedure to evaluate model tests. It combines various aspects of resistance, propulsion, and open-water tests. These are comprehensively reviewed here. Further details may be found in Section 3.2.5, Section 3.2.7, and Section 2.5, Chapter 2. The IPPM78 assumes that the following tests have been performed yielding the corresponding results:

resistance test $R_{Tm} = f(V_m)$
open-water test $T_m = f(V_{Am}, n_m)$

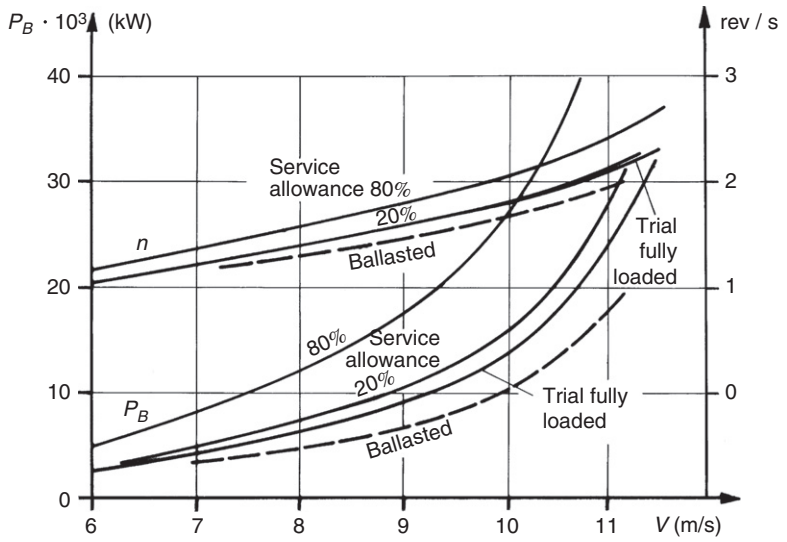

Figure 3.9:
Result of propulsion test

$$Q_m = f(V_{Am}, n_m)$$

propulsion test $T_m = f(V_m, n_m)$

$$Q_m = f(V_m, n_m)$$

R_T is the total resistance, V the ship speed, V_A the average inflow speed to the propeller, n the propeller rpm, K_T the propeller thrust coefficient, and K_Q the propeller torque coefficient. Generally, m denotes model, s full scale.

The resistance is evaluated using the ITTC 1978 method (for single-screw ships) described in Section 3.2.5:

1. Determine the total resistance coefficient in the model test:

$$c_{Tm} = \frac{R_{Tm}}{\frac{1}{2}\rho_m V_m^2 S_m} \tag{3.33}$$

2. Determine the frictional resistance coefficient for the model following ITTC 1957:

$$c_{Fm} = \frac{0.075}{(\log_{10} R_{nm} - 2)^2} \tag{3.34}$$

The Reynolds number of the model is $R_{nm} = V_m L_{osm}/\nu_m$, where L_{os} is the wetted length of the model. L_{os} is the length of the overall wetted surface, i.e. usually the length from the tip of the bulbous bow to the trailing edge of the rudder.

3. Determine the wave resistance coefficient, same for model and ship:

$$c_w = c_{Tm} - (1 + k)c_{Fm} \tag{3.35}$$

The determination of the form factor $(1 + k)$ is described below.

4. Determine the total resistance coefficient for the ship:

$$c_{Ts} = c_w - (1 + k)c_{Fs} + c_A + c_{AA} \tag{3.36}$$

c_{Fs} is the frictional resistance coefficient following ITTC 1957, but for the full-scale ship. c_A is a correlation coefficient (roughness allowance). c_{AA} considers the air resistance:

$$c_A = \left(105\sqrt[3]{\frac{k_s}{L_{oss}}} - 0.64\right) \cdot 10^{-3} \tag{3.37}$$

k_s is the roughness ($= 1.5 \cdot 10^{-4}$ m) and L_{oss} the wetted length of the ship.

$$c_{AA} = 0.001\frac{A_T}{S_s} \tag{3.38}$$

A_T is the frontal area of the ship above the water, S_s the wetted surface.

5. Determine the total resistance for the ship:

$$R_{Ts} = c_{Ts} \cdot \frac{1}{2}\rho_s V_s^2 S_s \tag{3.39}$$

The form factor is determined in a least square fit of α and n in the function:

$$\frac{c_{Tm}}{c_{Fm}} = (1 + k) + \alpha \cdot \frac{F_n^n}{c_{Fm}} \tag{3.40}$$

The open-water test gives the thrust coefficient K_T and the torque coefficient K_Q as functions of the advance number J:

$$K_{Tm} = \frac{T_m}{\rho_m n_m^2 D_m^4} \qquad K_{Qm} = \frac{Q_m}{\rho_m n_m^2 D_m^5} \qquad J = \frac{V_{Am}}{n_m D_m} \tag{3.41}$$

D_m is the propeller diameter. The model propeller characteristics are transformed to full scale (Reynolds number correction) as follows:

$$K_{Ts} = K_{Tm} + 0.3 \cdot Z \cdot \frac{c}{D_s} \cdot \frac{P_s}{D_s} \cdot \Delta C_D \tag{3.42}$$

$$K_{Qs} = K_{Qm} - 0.25 \cdot Z \cdot \frac{c}{D_s} \cdot \Delta C_D \tag{3.43}$$

Z is the number of propeller blades, P_s/D_s the pitch−diameter ratio, D_s the propeller diameter in full scale, and c the chord length at radius $0.7D$.

$$\Delta C_D = C_{Dm} - C_{Ds} \tag{3.44}$$

This is the change in the profile resistance coefficient of the propeller blades. These are computed as:

$$C_{Dm} = 2\left(1 + 2\frac{t_m}{c_m}\right)\left(\frac{0.044}{R_{nco}^{1/6}} - \frac{5}{R_{nco}^{2/3}}\right) \tag{3.45}$$

t is the maximum blade thickness, c the maximum chord length. The Reynolds number $R_{nco} = V_{co}c_m/\nu_m$ at $0.7D_m$, i.e. $V_{co} = \sqrt{V_{Am}^2 + (0.7\pi n_m D_m)^2}$.

k_p is the propeller blade roughness, taken as $3 \cdot 10^{-5}$ if not otherwise known.

The evaluation of the propulsion test requires the resistance and open-water characteristics. The open-water characteristics are denoted here by the index *fv*. The results of the propulsion test are denoted by *pv*:

$$C_{Ds} = 2\left(1 + 2\frac{t_s}{c_s}\right)\left(1.89 + 1.62\log_{10}\frac{c_s}{k_p}\right)^{-2.5} \tag{3.46}$$

Thrust identity is assumed, i.e. $K_{Tm,pv} = K_{Tm,fv}$. Then the open-water diagram can be used to determine the advance number J_m. This in turn yields the wake fraction of the model:

$$w_m = 1 - \frac{J_m D_m n_m}{V_m} \tag{3.47}$$

The thrust deduction fraction is:

$$t = 1 + \frac{F_D - R_{Tm}}{T_m} \tag{3.48}$$

F_D is the force compensating for the difference in resistance similarity between model and full-scale ship:

$$F_D = \frac{1}{2}\rho \cdot V_m^2 \cdot S \cdot ((1+k)(c_{Fm} - c_{Fs}) - c_A - c_{AA}) \tag{3.49}$$

With known J_m the torque coefficient $K_{Qm,fv}$ can also be determined. The propeller efficiency behind the ship is then:

$$\eta_{bm} = \frac{K_{Tm,pv}}{K_{Qm,pv}} \cdot \frac{J_m}{2\pi} \tag{3.50}$$

The open-water efficiency is:

$$\eta_{0m} = \frac{K_{Tm,fv}}{K_{Qm,fv}} \cdot \frac{J_m}{2\pi} \tag{3.51}$$

This determines the relative rotative efficiency:

$$\eta_R = \frac{\eta_{bm}}{\eta_{0m}} = \frac{K_{Qm,fv}}{K_{Qm,pv}} \cdot \frac{K_{Tm,fv}}{K_{Tm,fv}} \tag{3.52}$$

While t and η_R are assumed to be the same for ship and model, the wake fraction w has to be corrected:

$$w_s = w_m \frac{c_{Fs}}{c_{Fm}} + (t + 0.04)\left(1 - \frac{c_{Fs}}{c_{Fm}}\right) \tag{3.53}$$

A curve for the parameter K_T/J^2 as function of J is introduced in the open-water diagram for the full-scale ship. The design point is defined by:

$$\left(\frac{K_T}{J^2}\right)_s = \frac{T_s}{\rho_s \cdot D_s^2 \cdot V_{As}^2} = \frac{S_s}{2D_s^2} \cdot \frac{c_{Ts}}{(1-t)(1-w_s)^2} \tag{3.54}$$

The curve for K_T/J^2 can then be used to determine the corresponding J_s. This in turn determines the torque coefficient of the propeller behind the ship $K_{Qs} = f(J_s)$ and the open-water propeller efficiency $\eta_{0s} = f(J_s)$. The propeller rpm of the full-scale propeller is then:

$$n_s = \frac{(1-w_s) \cdot V_s}{J_s \cdot D_s} \tag{3.55}$$

The propeller torque in full scale is then:

$$Q_s = \frac{K_{Qs}}{\eta_R} \rho_s \cdot n_s^2 \cdot D_s^2 \tag{3.56}$$

The propeller thrust of the full-scale ship is:

$$T_s = \left(\frac{K_T}{J^2}\right)_s \cdot J_s^2 \cdot \rho_s \cdot n_s^2 \cdot D_s^4 \tag{3.57}$$

The delivered power is then:

$$P_{Ds} = Q_s \cdot 2\pi \cdot n_s \tag{3.58}$$

The total propulsion efficiency is then:

$$\eta_{Ds} = \eta_0 \cdot \eta_R \cdot n_{Hs} \tag{3.59}$$

3.3. Additional Resistance Under Service Conditions

The model test conditions differ in certain important points from trial and service conditions for the real ship. These include effects of:

- appendages;
- shallow water;
- wind;
- roughness;
- seaway.

Empirical corrections (based on physically more or less correct assumptions) are then used to estimate these effects and to correlate measured values from one state (model or trial) to another (service). The individual additional resistance components will be briefly discussed in the following.

- Appendages
  Model tests can be performed with geometrically properly scaled appendages. However, the flow around appendages is predominantly governed by viscous forces and would require Reynolds similarity. Subsequently, the measured forces on the appendages for Froude similarity are not properly scaled up to the real ship. Appendages may be tested separately and often the resistance of the appendages is scaled separately and added in a prediction for the full-scale ship. Unfortunately, this procedure does not account for interaction between hull and appendages and also introduces considerable error margins. Fortunately, most ships have only a few appendages and errors in estimating their resistance can be accepted. For unconventional ships with many and complex appendages, the difficulties in estimating the resistance of the appendages properly leads to a larger margin of uncertainty for the global full-scale prediction.
  Schneekluth and Bertram (1998) compiled some data from shipbuilding experience:
  - Properly arranged bilge keels contribute only 1−2% to the total resistance of ships. However, trim and ship motions in seastates increase the resistance more than for ships without bilge keels. Thus, in evaluation of model tests, a much higher increase of resistance should be made for ships in ballast condition.
  - Bow thrusters, if properly designed and located, do not significantly increase resistance. Transverse thrusters in the aftbody may increase resistance by 1−6%.
  - Shaft brackets and bossings increase resistance by 5−12%. For twin-screw ships with long propeller shafts, the resistance increase may be more than 20%.
  - Rudders increase resistance little (~1%) if in the neutral position and improve propulsion. But moderate rudder angles may increase resistance already by 2−6%.
- Shallow water
  Shallow water increases friction resistance and usually also wave resistance. Near the critical depth Froude number $F_{nh} = 1$, the resistance is strongly increased. Figure 3.10

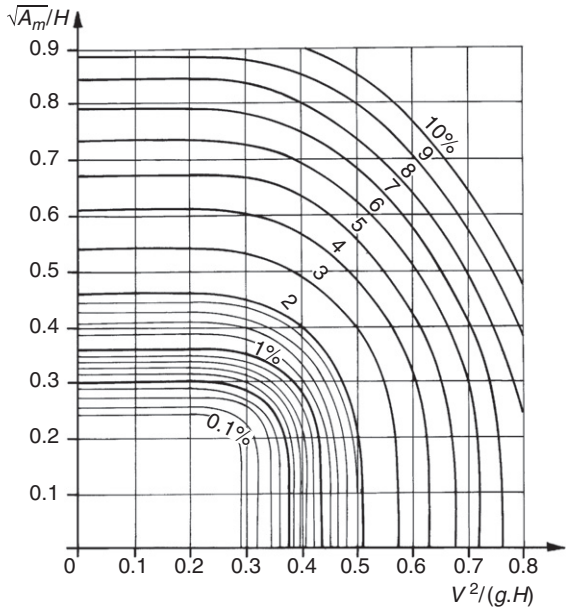

Figure 3.10:
Percentage loss of speed in shallow water (Lackenby 1963); A_m = midship section area, H = water depth, $V^2/(gH) = F_{nh}^2$

allows estimating the speed loss for weak shallow-water influence. The figure follows Schlichting's hypothesis that the wave resistance is the same if the wave lengths of the transversal waves are the same. Similar, but more sophisticated, diagrams are still popular in practice. For strong shallow-water influence, a simple correction is impossible as wave-breaking, squat and deformation of the free surface introduce complex physical interactions. In this case, only model tests or CFD may help.

In numerical simulations (CFD), the inclusion of shallow water is relatively simple. Boundary element methods based on Rankine elements use mirror images of the elements with respect to the water bottom. The image elements have the same strength as the original elements. This automatically yields zero normal velocity on the water bottom due to symmetry. The analytical inclusion of the bottom in Green function methods is more difficult, but also feasible. Field methods discretize the fluid domain to the water bottom and enforce a suitable boundary condition there. Shallow-water flows often feature stronger non-linearities than deep-water flows, making them in turn more difficult to solve numerically. CFD is much better suited to predict squat (dynamic trim and sinkage) in restricted waters than empirical formulae or even model tests.

- Wind
  Wind resistance is important for ships with large lateral areas above the water level, e.g. container ships and car ferries. Fast and unconventional ships, e.g. air-cushioned vehicles,

also require the contribution of wind or air resistance. Schneekluth and Bertram (1998) give simple design estimates with empirical formulae. Usually wind tunnel tests are the preferred choice for a more accurate estimate, as they are fast and cheap to perform. CFD is not yet competitive, as grid generation is so far too time-consuming and expensive for most applications. However, several prototype applications have shown the capability of CFD to compute air flow about complex ship and offshore geometries with good results. As costs for grid generation will decrease, CFD may also increasingly substitute for wind tunnel tests.

- Roughness
  The friction resistance can increase considerably for rough surfaces. For new ships, the effect of roughness is included in the ITTC line or the correlation constant. The problem of correlating roughness and resistance is insufficiently understood. Model tests try to produce a hull surface as smooth as possible. As a rule, CFD does not consider roughness at all. Coating roughness is best defined by the average maximum peak-to-trough in a 50 mm sample length, measured along the hull surface (Swain 2010). This value can be measured using a hull roughness analyzer instrument. The mean roughness is obtained by making typically 10–15 of these measurements in one pass. It is recommended that at least 100 locations distributed around the hull are measured and the values combined to get an average hull roughness (AHR) value. The AHR can then be used to correct the resistance coefficient, following ITTC (1990):

$$\Delta c_f = \left(44 \left[\sqrt[3]{\frac{AHR}{L}} - 10 R_n^{-1/3} \right] + 0.125 \right) \cdot 10^{-3} \tag{3.60}$$

This formula is valid for coatings with roughness values up to 225 microns. According to this formula, a rough hull surface (without fouling) may increase the frictional resistance by up to 5%. Fouling can increase the resistance by much more. Swain (2010) gives an example for the required power increase for a frigate at 15 knots, using the Naval Ships' Technical Manual (NSTM) rating:

NSTM rating	Description	Increase in required power
0	Hydraulically smooth surface	0%
0	Typical as applied antifouling coating	2%
10–20	Deteriorated coating or light slime	11%
30	Heavy slime	21%
40–60	Small calcareous fouling or weed	35%
70–80	Medium calcareous fouling	54%
90–100	Heavy calcareous fouling	86%

Fouling is estimated to be a serious problem. Munk and Kane (2009) found (based on statistical data of 10 years) that some 20% of the world's fleet are in poor condition with added resistance due to fouling in excess of 50% of the total resistance.

- Seaway
  The added resistance of a ship in a seaway is generally determined by computational methods and will be discussed in more detail in the chapters treating ship seakeeping. Such predictions for a certain region or route depend on the accuracy of seastate statistics, which usually introduce a larger error than the actual computational simulation. Ship size is generally more important than ship shape. Schneekluth and Bertram (1998) give simple design estimates for the speed loss due to added resistance in waves.

3.4. Fast Ships

3.4.1. Fast Monohulls

Most fast monohulls operate at Froude numbers $0.3 < F_n < 1.7$. There is a considerable overlap in operational speed ranges for various fast ship hull forms, but care should be taken in selecting the appropriate hull form. For example, planing hulls operated at $F_n < 0.6$ require more power than round-bilge non-planing hulls of the same displacement.

The most common representatives of fast monohulls are:

- *Displacement ships*. Typical examples are corvettes, frigates, and working boats. The hulls are characterized by straight V-shaped sections in the forebody, slender waterlines, round bilge with decreasing radius going to the transom stern and centerline skeg. They are frequently fitted with an integrated trim wedge. The LCB (longitudinal center of buoyancy) positions usually lie between 2% and 3% aft of $L_{pp}/2$ for larger ships. Displacement ships operate up to $F_n = 0.4{-}0.6$, i.e. they approach only the beginning of the planing condition. Advantages of this hull form are good seakeeping behavior, good course-keeping ability, and – if the vessel operates above the resistance hump – relatively low dynamic trim at top speed. The steep run of the power curve at higher speeds, caused by the fact that little hydrodynamic lift is produced, is the main disadvantage and determines the operational limits of this type.
- *Semi-displacement ships*. Typical examples are patrol boats, special navy craft, pleasure yachts, pilot boats, etc. Semi-displacement ships achieve higher speeds than displacement ships due to increased dynamical lift and corresponding reduction in resistance. Vessels can reach the planing condition with speeds of up to $F_n \approx 1$. The course-changing and course-keeping behavior is similar to that of pure displacement ships. The seakeeping is in general good. At high speeds, roll-induced transverse instability can arise under certain circumstances.

- *Planing hulls*. Typical examples are fast patrol boats, racing boats, search and rescue boats, and fast small passenger ferries. Planing hull designs should normally be used for high-speed vessels only. The stations have straight sections and knuckle lines (with a bilge knuckle running from the stem over the entire length to the transom), relatively large deadrise angles in the forebody decreasing further aft to approximately $L/2$ and continuing at nearly constant angles of not less than 10° to the transom. Early planing hull designs with warped deadrise are not common today. The forward part of the longitudinal knuckle is designed to work as a spray rail. Trim wedges with adjustable tabs are often installed to control the dynamic trim. These become less effective for $F_n > 1$ as there is generally a reduction in dynamic trim in that speed range. The typical advantages of this hull form develop at speeds $F_n > 1$. The seakeeping qualities of these vessels are not as good as for displacement and semi-displacement hulls. This disadvantage can be partially compensated by selecting relatively high L/B ($L/B \approx 7-8$) and deadrise angles $\tau > 10^\circ$ in the aft part. The high-speed stability problem of semi-displacement hulls may also occur with planing hulls.

The power requirements of fast ships can be estimated following Bertram and Mesbahi (2004), who derived formulae based on graphs given by Fritsch and Bertram (2002). The resistance of high-speed vessels is primarily a function of the vessel's displacement, wetted length and surface, speed and additionally breadth for planing hulls. Therefore significant parameters are the slenderness $L/\nabla^{1/3}$ and the specific resistance R_T/∇. The total resistance R_T is decomposed as usual:

$$R_T = R_F + R_R \tag{3.61}$$

$$R_F = c_F \cdot \frac{\rho}{2} \cdot V^2 \cdot S \tag{3.62}$$

$$R_R = R_W + R_{APP} + R_{AA} + R_{PARAS} \tag{3.63}$$

The wetted surface S is defined at rest except for planing hulls as described in more detail below; c_F follows ITTC'57 with Reynolds number based on L_{wl}. The appendage resistance R_{APP}, the air and wind resistance R_{AA}, and the parasitic resistance R_{PARAS} (resistance of hull openings such as underwater exhaust gas exits, scoops, zinc anodes, etc.) can be estimated globally with 3–5% R_F for a projected vessel, but the determination of R_R (which includes wave, wave-making, spray and viscous pressure or separation resistance) is more difficult. It is common practice to take data from one of the systematical series, e.g. Bailey (1976) or Blount and Clement (1963). However, these prediction methods are time-consuming and semi-empirical formulae are more helpful for design engineers.

R_{AA} can be calculated following empirical formulae given in Section 3.6.

Considering the propulsive efficiencies yields the necessary engine power P_B from the effective power P_E:

$$P_B = \frac{P_E}{\eta_D \cdot \eta_M} \tag{3.64}$$

$\eta_M = 95\%$ is a typical mechanical efficiency of gearbox and shaft bearings. The propulsive efficiency is $\eta_D = \eta_H \cdot \eta_R \cdot \eta_0$. Since $\eta_H \approx 1$ and $\eta_R \approx 1$ for these hull forms, the main influence is the propeller efficiency η_0. Modern propeller designs and waterjet propulsion systems can reach values of more than 70% under good operational conditions.

The power may be predicted for conventional fast ships as follows:

- *Planing hulls*. Different test series are available for the necessary reliable power prediction in the early design phase. The most useful is the DTMB Series 62 (Blount and Clement 1963). More recently, HSVA formulae offer a simple estimate (Fritsch and Bertram 2002):

$$P_B = 0.7354 \cdot \left(\frac{\Delta \cdot V}{765.2} + \frac{B_C^2 \cdot V^3}{1051.1} \right) \tag{3.65}$$

  B_C [m] is the mean of the maximum beam at chines and the chine beam at the transom. V [kn] is the speed and P_B [kW] the brake power. B_C can be estimated in the design stage by:

$$B_C = 0.215 \cdot \Delta^{0.275} \tag{3.66}$$

  Δ [t] is the displacement mass.
- *Semi-displacement hulls*. The procedure for estimating resistance and power is very similar as for planing hulls. The NPL High Speed Round Bilge Displacement Hull Series (Bailey 1976) is available to aid the selection of main dimensions, lines design, resistance, and power prediction. This series also deals with examples for practical application. A simple estimate following HSVA is (Bertram and Mesbahi 2004):

$$R_T = C_{T\nabla} \cdot \frac{\rho}{2} \cdot V^2 \cdot \nabla^{2/3} \tag{3.67}$$

  $C_{T\nabla}$ is a function of the Froude number, given by the following relations:

  For $0.002 < C_{T\nabla} < 0.005$, $0.4 < F_n < 1.2$:

$$\begin{aligned} C_{T\nabla} = c_0 + c_1 \cdot \mathrm{sig}\,[b_0 + b_1 \cdot \mathrm{sig}(a_{10} + a_{11} \cdot x_1 + a_{12} \cdot x_2) \\ + b_2 \cdot \mathrm{sig}(a_{20} + a_{21} \cdot x_1 + a_{22} \cdot x_2) + b_3 \cdot \mathrm{sig}(a_{30} + a_{31} \cdot x_1 + a_{32} \cdot x_2) \\ + b_4 \cdot \mathrm{sig}(a_{40} + a_{41} \cdot x_1 + a_{42} \cdot x_2) + b_5 \cdot \mathrm{sig}(a_{50} + a_{51} \cdot x_1 + a_{52} \cdot x_2)] \end{aligned} \tag{3.68}$$

$$x_1 = 1.125 \cdot F_n - 0.4 \quad x_2 = 0.299 \cdot C_{T\nabla} - 0.5481$$
$$a_{10} = 0.07700 \quad a_{11} = -5.28009 \quad a_{12} = 1.58541$$
$$a_{20} = -4.15170 \quad a_{21} = -4.40526 \quad a_{22} = 1.49122$$
$$a_{30} = 0.49661 \quad a_{31} = 2.49719 \quad a_{32} = -5.00270$$
$$a_{40} = -12.78673 \quad a_{41} = 13.63660 \quad a_{42} = -0.00639$$
$$a_{50} = 1.38547 \quad a_{51} = -29.74828 \quad a_{52} = -0.04912$$
$$b_0 = -1.04511 \quad b_1 = 5.51238 \quad b_2 = -0.98215$$
$$b_3 = -2.13594 \quad b_4 = 4.56969 \quad b_5 = -6.46482$$
$$c_0 = 0.02688 \quad c_1 = 0.0522$$

For $0.0025 < C_{T\nabla} < 0.007$, $0.2 < F_n < 0.45$:

$$\begin{aligned} C_{T\nabla} = c_0 + c_1 \cdot \text{sig}\,[&b_0 + b_1 \cdot \text{sig}(a_{10} + a_{11} \cdot x_1 + a_{12} \cdot x_2) \\ &+ b_2 \cdot \text{sig}(a_{20} + a_{21} \cdot x_1 + a_{22} \cdot x_2) \\ &+ b_3 \cdot \text{sig}(a_{30} + a_{31} \cdot x_1 + a_{32} \cdot x_2) \\ &+ b_4 \cdot \text{sig}(a_{40} + a_{41} \cdot x_1 + a_{42} \cdot x_2)] \end{aligned} \tag{3.69}$$

$$x_1 = 3 \cdot F_n - 0.55 \quad x_2 = 0.1992 \cdot C_{T\nabla} - 0.44642$$
$$a_{10} = 2.47120 \quad a_{11} = -4.70440 \quad a_{12} = -0.71328$$
$$a_{20} = 2.80191 \quad a_{21} = -5.08604 \quad a_{22} = -0.80876$$
$$a_{30} = 0.53110 \quad a_{31} = -2.42700 \quad a_{32} = -0.61778$$
$$a_{40} = 0.15070 \quad a_{41} = 0.85700 \quad a_{42} = 0.72333$$
$$b_0 = 0.89195 \quad b_1 = -1.74315 \quad b_2 = -1.91516$$
$$b_3 = -0.80806 \quad b_4 = 0.60328$$
$$c_0 = 0.019134 \quad c_1 = 0.05333$$

For frigates and corvettes, for $0.0016 < C_{T\nabla} < 0.0029$, $0.25 < F_n < 0.8$:

$$\begin{aligned} C_{T\nabla} = c_0 + c_1 \cdot \text{sig}\,[&b_0 + b_1 \cdot \text{sig}(a_{10} + a_{11} \cdot x_1 + a_{12} \cdot x_2) \\ &+ b_2 \cdot \text{sig}(a_{20} + a_{21} \cdot x_1 + a_{22} \cdot x_2) + b_3 \cdot \text{sig}(a_{30} + a_{31} \cdot x_1 + a_{32} \cdot x_2) \\ &+ b_4 \cdot \text{sig}(a_{40} + a_{41} \cdot x_1 + a_{42} \cdot x_2) + b_5 \cdot \text{sig}(a_{50} + a_{51} \cdot x_1 + a_{52} \cdot x_2)] \end{aligned} \tag{3.70}$$

$$x_1 = 1.636 \cdot F_n - 0.359 \quad x_2 = 0.75541 \cdot C_{T\nabla} - 1.1959$$
$$a_{10} = -5.38402 \quad a_{11} = 16.26584 \quad a_{12} = -0.6375$$
$$a_{20} = -2.84961 \quad a_{21} = 9.28172 \quad a_{22} = -1.9176$$
$$a_{30} = -3.62339 \quad a_{31} = -4.52883 \quad a_{32} = 6.16248$$
$$a_{40} = 1.91471 \quad a_{41} = -3.14575 \quad a_{42} = 2.17611$$
$$a_{50} = 0.93425 \quad a_{51} = -11.05182 \quad a_{52} = 1.45755$$
$$b_0 = -1.1453 \quad b_1 = 3.40313 \quad b_2 = -3.32619$$
$$b_3 = 1.88172 \quad b_4 = 1.22925 \quad b_5 = -3.5398$$
$$c_0 = 0.01331 \quad c_1 = 0.04177$$

Since the value found for the effective power is valid for the bare hull only, allowances for R_{APP} and R_{AA} must be added. R_{APP} can be calculated directly, e.g. Bailey (1976), or estimated from statistical data:

Two propellers:

$$R_{APP}/R_T\ [\%] = c_0 + c_1 \cdot \text{sig}\ [b_0 + b_1 \cdot \text{sig}(a_{10} + a_{11} \cdot x_1) + b_2 \cdot \text{sig}(a_{20} + a_{21} \cdot x_1)] \quad (3.71)$$

$$\begin{aligned} x_1 &= 0.6544 \cdot F_n + 0.0338 \\ a_{10} &= -7.3461 \quad a_{11} = 14.1181 \quad a_{20} = -3.5455 \quad a_{21} = 13.3944 \\ b_0 &= 2.9959 \quad b_1 = 4.0700 \quad b_2 = -6.8369 \\ c_0 &= 7.0235 \quad c_1 = 8.7183 \end{aligned}$$

Three propellers:

$$R_{APP}/R_T\ [\%] = c_0 + c_1 \cdot \text{sig}\ [b_0 + b_1 \cdot \text{sig}(a_{10} + a_{11} \cdot x_1) + b_2 \cdot \text{sig}(a_{20} + a_{21} \cdot x_1)] \quad (3.72)$$

$$\begin{aligned} x_1 &= 0.6453 \cdot F_n + 0.0477 \\ a_{10} &= -4.231 \quad a_{11} = 15.0686 \quad a_{20} = -7.375 \quad a_{21} = 14.0019 \\ b_0 &= 2.7373 \quad b_1 = -6.4811 \quad b_2 = 4.0462 \\ c_0 &= 10.7197 \quad c_1 = 12.5462 \end{aligned}$$

Four propellers:

$$R_{APP}/R_T\ [\%] = c_0 + c_1 \cdot \text{sig}\ [b_0 + b_1 \cdot \text{sig}(a_{10} + a_{11} \cdot x_1) + b_2 \cdot \text{sig}(a_{20} + a_{21} \cdot x_1)] \quad (3.73)$$

$$\begin{aligned} x_1 &= 0.6859 \cdot F_n - 0.007964 \\ a_{10} &= 3.7972 \quad a_{11} = -16.4323 \quad a_{20} = 5.9647 \quad a_{21} = -11.98701 \\ b_0 &= 0.3437 \quad b_1 = 6.2153 \quad b_2 = -3.7455 \\ c_0 &= 14.2334 \quad c_1 = 16.4206 \end{aligned}$$

These formulae do not include interference effects from the individual parts of the appendages.

Appendages play a special role for fast ships. Many fast displacement, semi-displacement, and also planing hulls are characterized by moderate to severe spray generation. The spray comes from the bow wave rising up the hull with speed. This is particularly caused by the relatively blunt waterlines and hard buttock forward when $L/\nabla^{1/3}$ is unfavorably small or the beam too large. Severe spray generation has a number of disadvantages:

- The increase of frictional (due to larger wetted surface) and wave-making resistance.
- Wetness of deck and superstructures, unfavorable for yachts and unacceptable for gas turbine-powered ships (due to their demand for very dry and salt-free combustion air).
- Increased radar signature (for navy craft).

Spray generation can be taken into account when designing the hull before entering the construction phase. Sometimes hull changes are not possible. Then spray rails can often be an effective and relatively cheap measure to reduce spray generation. Spray rails can also improve

the performance of existing fast ships. Typical spray rail arrangements either use an additional triangular profile or integrate a two-step knuckle line into the form. These run from the stem to about amidships. In both cases a horizontal deflection area with a sharp edge must be created. Spray rails also influence the dynamic lift on the forebody, thus improving the resistance also indirectly.

The resistance of a fast ship is fundamentally linked with the dynamic trim. Recommended optimum trim angles for fast vessels in modern practice according to HSVA are (Bertram and Mesbahi 2004):

Displacement and semi-displacement hulls

$$\begin{aligned}\theta = 0.7 \cdot \{c_0 + c_1 \cdot \text{sig}\,[b_0 &+ b_1 \cdot \text{sig}(a_{10} + a_{11} \cdot x_1 + a_{12} \cdot x_2) \\ &+ b_2 \cdot \text{sig}(a_{20} + a_{21} \cdot x_1 + a_{22} \cdot x_2) \\ &+ b_3 \cdot \text{sig}(a_{30} + a_{31} \cdot x_1 + a_{32} \cdot x_2) \\ &+ b_4 \cdot \text{sig}(a_{40} + a_{41} \cdot x_1 + a_{42} \cdot x_2)]\}\end{aligned} \tag{3.74}$$

$$\begin{aligned} x_1 &= 0.9 \cdot \left(\nabla^{2/3}/B \cdot T\right) - 1.975 \quad x_2 = 0.71 \cdot F_n - 0.0795 \\ a_{10} &= -3.75198 \quad a_{11} = -1.69432 \quad a_{12} = 9.49288 \\ a_{20} &= -2.49216 \quad a_{21} = 3.86243 \quad a_{22} = -1.65272 \\ a_{30} &= 3.87188 \quad a_{31} = 0.61239 \quad a_{32} = -17.00609 \\ a_{40} &= -2.68088 \quad a_{41} = -3.55418 \quad a_{42} = 3.42624 \\ b_0 &= 1.63558 \quad b_1 = -2.18713 \quad b_2 = 2.15603 \\ b_3 &= -4.84437 \quad b_4 = -1.51677 \\ c_0 &= -0.17276 \quad c_1 = 2.364 \end{aligned} \tag{3.75}$$

B is the width, T the draft, ∇ the volumetric displacement.

Planing hulls

$$\begin{aligned}\theta = 0.7 \cdot \{c_0 + c_1 \cdot \text{sig}\,[b_0 &+ b_1 \cdot \text{sig}(a_{10} + a_{11} \cdot x_1 + a_{12} \cdot x_2) \\ &+ b_2 \cdot \text{sig}(a_{20} + a_{21} \cdot x_1 + a_{22} \cdot x_2)]\}\end{aligned}$$

$$\begin{aligned} x_1 &= 0.6 \cdot (\nabla^{2/3}/B \cdot T) - 0.85 \quad x_2 = 0.6624 \cdot F_n - 0.01936 \\ a_{10} &= -2.66906 \quad a_{11} = 0.12856 \quad a_{12} = 8.06127 \\ a_{20} &= 6.30112 \quad a_{21} = -3.37513 \quad a_{22} = -3.66594 \\ b_0 &= -0.83869 \quad b_1 = 4.16294 \quad b_2 = -2.71566 \\ c_0 &= -0.39046 \quad c_1 = 6.535 \end{aligned}$$

Fixed trim wedges or moveable trim flaps can be used to optimize the dynamic trim for a given speed and slenderness. Trim wedges should normally be considered during the design phase, but they are also acceptable for improving craft already in service. Trim wedges are most effective at speeds in the resistance hump range at $F_n \approx 0.4{-}0.5$. They have almost no effect for $F_n > 1.2$. Reductions in total resistance of more than 10% are possible in the resistance hump range. The most effective trim wedge for a certain craft and operational range is best found in model tests.

Fixed or adjustable interceptors offer an alternative to control the dynamic trim of a vessel. An interceptor is basically a vertical extension of the transom beyond the shell plating. Forward of the interceptor plate the flow is decelerated and the local pressure is increased which generates a lift force to the vessel's stern. The effect is identical to that of a conventional stern wedge. However, the height of the interceptor needs only to be 50% of that of a wedge for the same effect on the dynamic trim and resistance. This is an advantage at lower speed due to the smaller immersed transom area.

Appendages strongly influence resistance and propulsive efficiency of fast ships ($R_{APP} = 6-15\%$ R_T). Recommendations are:

- Avoid over-sizing the shaft brackets, bossings, and rudder profiles.
- V-bracket designs may have approximately 5−7% higher R_{APP} than I-bracket designs.
- If V-brackets are obligatory for whatever reason the inner and outer legs should be aligned with the flow to minimize resistance and wake disturbance (vibration, cavitation). Optimization of the brackets may employ CFD or model tests (three-dimensional wake measurements).
- For twin-screw vessels, power consumption may differ by 3−5%, changing the sense of propeller rotation, depending on the aftbody lines. The propulsive coefficient η_D is also influenced by the degree of shaft inclination ε, expressed by an additional efficiency η_ε, (Hadler 1966):

  $$\eta_\varepsilon = 1 - 0.00187 \cdot \varepsilon^{1.5} \tag{3.76}$$

  The decreasing tendency at increasing shaft angles ε indicates that the shaft arrangement should be considered carefully in the design. The phenomenon is due to the inhomogeneous flow to the propeller blades which reduces the propeller efficiency. Also cavitation may be increased to a certain degree.
- For twin-rudder arrangements, an inward inclination of the rudders' trailing edges by 2−3° can increase the propulsive efficiency by up to 3%.
- Strut barrels should be kept as small as possible and their noses should be rounded or have parabolic shapes.
- Bilge keels should generally be aligned with the flow at the bilge. The line of flow may be determined in paint tests or CFD.
- If non-retractable stabilizer fins are projected, the angle of attack with least resistance can be determined in model tests (with different adjusted fin angles) or employing CFD.

3.4.2. Catamarans

One of the advantages of catamarans vs. monohulls is the up to 70% larger deck area. On the other hand, catamarans have typically 20% more weight and 30−40% larger wetted surface. Catamarans usually require 20−80% (the higher values near $F_n = 0.5$) more power than monohulls due to higher frictional resistance and higher wave resistance. Catamarans feature

high transverse stability, but roll periods are similar to monohulls due to high moments of inertia. Catamaran designs come at low, medium and high speeds. Thus catamaran hull forms range from pure displacement up to real planing hulls.

Displacement catamarans usually operate near the hydrodynamically unfavorable hump speed ($F_n \approx 0.5$). The design is then usually driven by the demand for a large and stable working platform, high transverse stability and shallow draft where speed is not so important, e.g. for buoy layers, sight-seeing boats, etc. There is no typical hull form for displacement catamarans. Round bilge, hard chine, and combinations of both are used. Asymmetric hull forms are common to reduce the wave interference effects between the hulls. For catamarans with low design speed, a relatively large $L/\nabla^{1/3}$ should be selected to minimize the resistance. The majority of displacement catamarans are driven by fully immersed conventional propellers. Due to the frequent shallow draft requirements for catamarans the clearance for the propellers becomes rather small. Then arrangements of tunnels and propeller nozzles are usual.

Semi-displacement catamarans operate at higher speeds, frequently at the beginning of the planing condition at $F_n \approx 1$ or slightly above. Again, no typical hull characteristic is observed; both round-bilge and hard-chine sections are common. For rough seas (like the North Sea), round-bilge sections are more advantageous with respect to ride comfort. Most wave-piercer catamarans also have round-bilge sections. Semi-displacement catamarans may have propeller drives or waterjet propulsion.

Planing catamarans operate at speeds up to 50 knots or more and F_n up to 2.0 and higher. Typical knuckled planing hull forms dominate. Symmetric and asymmetric hull forms show only marginal performance differences. For high speeds, waterjets offer better efficiencies than conventional propellers with lower cavitation risk. Thus for planing catamarans, waterjets are the most favorable propulsion system. Surface-piercing propellers are also an option which has been employed by some racing boats and navy craft.

Foils may reduce resistance and improve seakeeping. Foil-assisted catamarans (FACs) have forward and aft foils, supporting part of the total weight. The bow is usually lifted clear of the water, but the stern remains partially immersed, which is necessary for waterjet operation and stability. Increasing the foil area decreases the resistance. For modern FACs, the foils are equipped with efficient ride control systems which usually adjust a movable flap on the forward foil and in more advanced systems also on the rear foils. Controllable flaps are recommended for several reasons. The risk of broaching in quartering or side waves can be reduced, especially when operating with foils in maximum lift condition. Controllable flaps also help to tune dynamical trim and foil adjustment for maximum lift and minimum resistance. For FACs, wetted length and surface of the model change very much with speed.

The highest stresses for fast catamarans are slamming impacts on the fore part of the wetdeck. The most common anti-slamming device (ASD) is a deep-V part in the forward wetdeck

above the calm waterline, as in wave-piercing catamarans. The wave energy in slamming events remains unchanged by ASDs, but is smeared over a longer period, thus reducing peaks. Arranging longitudinal rails and steps on the bottom of the wetdeck also reduces the slamming impacts as air–water cushions are formed between the longitudinal rails. Alternatively, longitudinal stiffeners with holes have been proposed.

The resistance for catamarans can be estimated following HSVA (Fritsch and Bertram 2002):

$$C_{T\nabla} = \frac{0.2}{L/\nabla^{1/3}} + \frac{2.05}{[1 + 25(F_n - 0.45)^2] \cdot (L/\nabla^{1/3})^2} \quad \text{round bilge} \tag{3.77}$$

$$C_{T\nabla} = \frac{0.25}{[1 + 25(F_n - 0.45)^2] \cdot (L/\nabla^{1/3})} + \frac{2.5}{[1 + 25(F_n - 0.45)^2] \cdot (L/\nabla^{1/3})^2} \quad \text{hard chine} \tag{3.78}$$

R_{APP} and R_{AA} must be added separately.

3.4.3. Problems for Fast and Unconventional Ships

Model testing has a long tradition for the prediction and optimization of ship performance of conventional ships. The scaling laws are well established and the procedures correlate model and ship with a high level of accuracy. The same scaling laws generally apply to high-speed craft, but two fundamental problems may arise:

1. Physical quantities may have major effects on the results which cannot be deduced from classical model tests. The physical quantities in this context are: surface tension (spray), viscous forces and moments, aerodynamic forces, cavitation.
2. Limitations of the test facilities do not allow an optimum scale. The most important limitations are generally water depth and carriage speed.

Fast and unconventional ships are often 'hybrid' ships, i.e. they produce the necessary buoyancy by more than one of the three possible options: buoyancy, dynamic lift (foils or planing), aerostatic lift (air cushion). For the propulsion of fast ships, subcavitating, cavitating, and ventilated propellers as well as waterjets with flush or pitot-type inlets are used. Due to viscous effects and cavitation, correlation to full-scale ships causes additional problems.

Generally we cannot expect the same level of accuracy for a power prediction as for conventional ships. The towing tank should provide an error estimate for each individual case. Another problem arises from the fact that the resistance curves for fast ships are often quite flat near the design point as are the curves of available thrust for many propulsors. For example, errors in predicted resistance or available thrust of 1% would result in an error of the attainable speed of also about 1%, while for conventional cargo ships the error in speed would often be only 1/3%, i.e. the speed prediction is more accurate than the power prediction.

The main problems for model testing are discussed individually:

- Model tank restrictions
  The physics of high-speed ships are usually highly non-linear. The positions of the ship in resistance (without propeller) and propulsion (with propeller) conditions differ strongly. Viscosity and free-surface effects, including spray and overturning waves, play significant roles, making both experimental and numerical predictions difficult.

  Valid predictions from tank tests for the resistance of the full-scale ship in unrestricted water are only possible if the tank is sufficiently large, as compared to the model to allow similarity in flow. Blockage, i.e. the ratio of the submerged cross-section of the model to the tank cross-section, will generally be very low for models of high-speed ships. However, shallow-water effects depend mainly on the model speed and the tank water depth. The depth Froude number F_{nh} should not be greater than 0.8 to be free of significant shallow-water effects.

  The frictional resistance is usually computed from the frictional resistance of a flat plate of similar length as the length of the wetted underwater body of the model. This wetted length at test speed differs considerably from the wetted length at zero speed for planing or semi-planing hull forms. In addition, the correlation requires that the boundary layer is fully turbulent. Even when turbulence stimulators are used, a minimum Reynolds number has to be reached. We can be sure to have a turbulent boundary layer for $R_n > 5 \cdot 10^6$. This gives a lower limit to the speeds that can be investigated depending on the model length used.

  Figure 3.11 illustrates, using a towing tank with water depth $H = 6$ m and a water temperature 15°C, how an envelope of possible test speeds evolves from these two restrictions. A practical

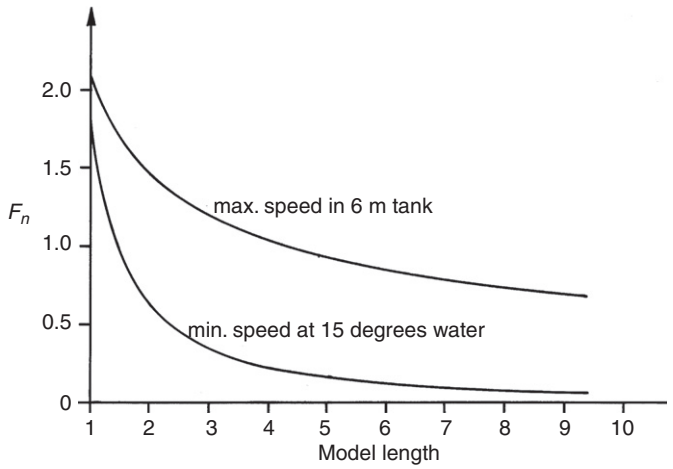

Figure 3.11:
Possible speed range to be safely investigated in a 6m deep towing tank at 15°C water temperature

limitation may be the maximum carriage speed. However, at HSVA the usable maximum carriage speed exceeds the maximum speed to avoid shallow-water effects.

- Planing hulls
  In the planing condition a significant share of the resistance is frictional and there is some aerodynamic resistance. At the design speed, the residual resistance, i.e. the resistance component determined from model tests, may only be 25−30% of the total resistance. In model scale, this part is even smaller. Therefore the measurements of the model resistance must be very accurate. Resistance of planing hulls strongly depends on the trim of the vessel. A careful test set-up is needed to ensure that the model is towed in the correct direction. The most important problem, however, is the accurate determination of the wetted surface and the wetted length which is needed to compute the frictional resistance for both the model and the ship. Side photographs, while popular, are not adequate. Preferably underwater photographs should be used. In many cases, the accurate measurement of trim and sinkage may be adequate in combination with hydrostatic computation of wetted surface and length. As the flotation line of such vessels strongly depends on speed, proper arrangement of turbulence stimulation is needed as well. Depending on the propulsion system, planing vessels will have appendages like rudders and shafts. For typical twin-screw ships with shafts, one pair of I-brackets and one pair of V-brackets, the appendage resistance could account for 10% of the total resistance of the ship. As viscous resistance is a major part of the appendage resistance and as the Reynolds number of the appendages will be small for the model in any case or the appendage may be within the boundary layer of the vessel, only a crude correlation of the appendage resistance is possible: the resistance of the appendage is determined in model scale by comparing the resistance of the model with and without appendages. Then an empirical correction for transferring the appendage resistance to the full-scale ship is applied. In many cases, it may be sufficient to perform accurate measurements without any appendages on the model and then use empirical estimates for the appendage resistance.
- Craft with hydrofoils
  Hydrofoils may be used to lift the hull out of the water to reduce resistance. Besides classical hydrofoil boats which are lifted completely out of the water and are fully supported by foil lift, hybrid hydrofoil boats may be used which are partially supported by buoyancy and partially by foil lift, e.g. catamarans with foils between the two hulls. When performing and evaluating resistance and propulsion tests for such vessels, the following problems have to be kept in mind:
  - The Reynolds number of the foils and struts will always be very low. Therefore the boundary layer on the foil may become partially laminar. This will influence the lift and the frictional resistance of the foils in a way requiring special correlation procedures to compensate at least partially for these scaling errors. The uncertainty level is still estimated as high as 5%, which is definitely higher than for conventional craft.

- Cavitation may occur on the full-scale hydrofoil. This will influence the lift and drag of the foils. Significant cavitation will certainly occur if the foil loading exceeds 10^5 N/m^2. With configurations not fully optimized for cavitation avoidance, significant cavitation is expected for foil loadings already in excess of $5 \cdot 10^4$ N/m^2. Another important parameter is the vessel's speed. Beyond 40 knots, cavitation has to be expected on joints to struts, flaps, foil tips, and other critical parts. At speeds beyond 60 knots, cavitation on the largest part of the foil has to be expected. When model testing these configurations in model tanks, no cavitation will occur. Therefore similarity of forces cannot be expected. To overcome this problem, resistance and propulsion tests could be performed in a free-surface cavitation tunnel. However, due to the usually small cross-sections of these tunnels, shallow-water effects may then be unavoidable. Therefore HSVA recommends the following procedure:

  1. Perform tests in the towing tank using non-cavitating foils from stock, varying angle of attack, and measure the total resistance and the resistance of the foils.
  2. Test the foils (including struts) in a cavitation tunnel varying angle of attack, observe cavitation and measure forces.
  3. Combine the results of both tests by determining the angle of attack for similar lift of foils and summing the resistance components.

  In the preliminary design phase, the tests in the cavitation tunnel may be substituted by corresponding flow computations. Alternatively, full-scale RANSE computations can be used.

- Surface effect ships (SES)
  SES combine aerostatic lift and buoyancy. The wave resistance curve of SES exhibits humps and hollows as in conventional ships. The magnitude of the humps and hollows in wave resistance depends strongly on the cushion L/B ratio. Wave-making of the submerged hulls and the cushion can simply be scaled according to Froude similarity as long as the tank depth is sufficient to avoid shallow-water effects. Otherwise a correction based on the potential flow due to a moving pressure patch is applied. Due to the significant influence of trim, this method has some disadvantages. To determine the wetted surface, observations inside the cushion are required with a video camera. The frictional resistance of the seals cannot be separated out of the total resistance. The pressure distribution between seals and cushion has to be controlled and the air flow must be determined. Also, the model aerodynamic resistance in the condition under the carriage has to be determined and used for separating the wave resistance. Generally separate wind tunnel tests are recommended to determine the significant aerodynamic resistance of such ships.
- Propulsion with propellers
  - *Conventional propellers.* Most of the problems concerning the scaling of resistance also appear in the propulsion test, as they determine the propeller loading. The use of a thrust deduction fraction is formally correct, but the change in resistance is partially due to a change of trim with operating propellers. For hydrofoils, the problem is that cavitation

is not present at model scale. Therefore, for cases with propeller loading where significant cavitation is expected, additional cavitation tests are used to determine the thrust loss due to cavitation. Z-drives which may even be equipped with contra-rotating propellers are expensive to model and to equip with accurate measuring devices. Therefore propulsion tests with such units are rarely performed. Instead the results of resistance and open-water tests of such units in a proper scale are numerically combined.

- *Cavitating propellers.* Certain high-speed propellers are designed to operate with a controlled extent of cavitation on the suction side of the blades. They are called super-cavitating or partially cavitating (Newton–Rader) propellers. These propulsors cannot be tested in a normal towing tank. Here again either resistance tests or propulsion tests with non-cavitating stock propellers are performed and combined with open-water tests in a cavitation tunnel.
- *Surface-piercing propellers.* Surface-piercing or ventilated propellers operate directly at the free surface. Thus the suction side is ventilated and therefore the collapse of cavitation bubbles on the blade surface is avoided. Due to the operation at the free surface, Froude similarity has to be maintained in model tests. On the other hand, thrust and torque, but more important also the side and vertical forces, strongly depend on the cavitation number. The vertical force may amount to up to 40% of the thrust and therefore will strongly influence the resistance of planing vessels or SES, ships where this type of propeller is typically employed.

- Waterjet propulsion
  A common means of propulsion for high-speed ships is the waterjet. Through an inlet in the bottom of the craft, water enters into a bent duct to the pump, where the pressure level is raised. Finally the water is accelerated and discharged in a nozzle through the transom. Power measurements on a model of the complete system cannot be properly correlated to full scale. Only the inlet and the nozzle are built to scale and an arbitrary model pump with sufficient capacity is used. The evaluation of waterjet experiments is difficult and usually involves several special procedures involving a combination of computations, e.g. the velocity profile on the inlet by boundary layer or RANSE computations, and measured properties, e.g. pressures in the nozzle. The properties of the pump are determined either in separate tests of a larger pump model, taken from experience with other pumps, or supplied by the pump manufacturer. A special committee of the ITTC was formed to cover waterjet propulsion and latest recommendation and literature references may be found in the ITTC proceedings.

3.5. CFD Approaches for Steady Flow

3.5.1. Wave Resistance Computations

The wave resistance problem considers the steady motion of a ship in initially smooth water assuming an ideal fluid, i.e. especially neglecting all viscous effects. The ship will create waves

at the freely deformable water surface. The computations involve far more information than the mere resistance, which is of minor importance in many applications and usually computed quite inaccurately. But the expression 'wave resistance problem' is easier than 'steady, inviscid straight-ahead course problem', and thus more popular.

The work of the Australian mathematician J. H. Michell in 1898 is often seen as the birth of modern theoretical methods for ship wave resistance predictions. While Michell's theory cannot be classified as computational fluid dynamics in the modern sense, it was a milestone at the time and is still inspiring mathematicians today. Michell expressed the wave resistance of a thin wall-sided ship as:

$$R_w = \frac{4}{\pi}\rho V^2 \nu_2 \int_1^\infty \frac{\lambda^2}{\sqrt{\lambda^2 - 1}} |A(\lambda)|^2 \, \mathrm{d}\lambda \tag{3.79}$$

with:

$$A(\lambda) = -i\nu\lambda \int_S \mathrm{e}^{\nu\lambda^2 z + i\nu\lambda x} f(x,z) \, \mathrm{d}z \, \mathrm{d}x \tag{3.80}$$

V is the ship speed, ρ water density, $\nu = g/V^2$, g gravity acceleration, $f(x,z)$ half-width of ship, x longitudinal coordinate (positive forward), z vertical coordinate (from calm waterline, positive upwards), and S ship surface below the calm waterline. The expression gives realistic results for very thin bodies (width/length ratio very small) for arbitrary Froude number, and for slender ships (width/length ratio and depth/length ratio very small) for high Froude numbers. Michell's theory (including all subsequent refinements) is in essence unacceptable for real ship geometries and ship speeds. However, on occasions it is still useful. An example may be the prediction of the wave resistance of a submarine near the free surface with a streamlined snorkel piercing the free surface. While CFD can discretize the main submarine, it will neglect all appendages of much smaller scale. Then Michell's theory can be applied to analyze the additional influence of the snorkel, which will have a very large Froude number based on the chord length of its profile cross-section. Söding (1995) gives a FORTRAN routine to compute Michell's integral.

The classical methods (thin ship theories, slender-body theories) introduce simplifications which imply limitations regarding the ship's geometry. Real ship geometries are generally not thin or slender enough. The differences between computational and experimental results are consequently unacceptable. Practical applications in industry are based largely on boundary element methods. These remain the most important design tools for naval architects despite the increasing application of viscous flow tools.

Classical methods using so-called Kelvin or Havelock sources fulfill automatically a crude approximation of the dynamical and kinematical free-surface conditions. Kelvin sources are complicated and require great care in their numerical evaluation. Rankine sources on the other

hand are quite simple. Wave resistance codes represent the flow as a superposition of Rankine sources and sometimes also dipoles or vortices. The potential of a Rankine point source is a factor divided by the distance between the point source and the considered point in the fluid domain. The factor is called the source strength. The derivative of the potential in an arbitrary spatial direction gives the velocity in this direction. This mathematical operation is simple to perform for Rankine sources.

Boundary element methods discretize surfaces into a finite number of elements and a corresponding number of collocation points. A desired (linear) condition is fulfilled exactly at these collocation points by proper adjustment of the initially unknown source strengths. One hopes/claims that between these points the boundary condition is fulfilled at least in good approximation. Laplace's equation and the decay condition (far away the ship does not disturb the flow) are automatically fulfilled. Mirror images of the panels at the bottom of the fluid domain walls may enforce a no-penetration condition there for shallow-water cases. Repeated use of mirror images at vertical canal walls can enforce in similar fashion the side-wall condition. For numerical reasons, this is preferable to a treatment of the side walls as collocation points similar as for the ship hull.

In the wave resistance problem, we consider a ship moving with constant speed V in water of constant depth and width. For inviscid and irrotational flow, this problem is equivalent to a ship being fixed in an inflow of constant speed. The following simplifications are generally assumed:

- Water is incompressible, irrotational, and inviscid.
- Surface tension is negligible.
- There are no breaking waves.
- The hull has no knuckles which cross streamlines.
- Appendages and propellers are not included in the model. (The inclusion of a propeller makes little sense as long as viscous effects are not also included.)

The governing field equation is Laplace's equation. A unique description of the problem requires further conditions on all boundaries of the modeled fluid domain:

- Hull condition: water does not penetrate the ship's surface.
- Transom stern condition: for ships with a transom stern, we generally assume that the flow separates and the transom stern is dry. Atmospheric pressure is then enforced at the edge of the transom stern. The condition is usually linearized assuming that the water flows only in the longitudinal direction. This can only approximately reflect the real conditions at the stern, but apparently works well as long as the transom stern is moderately small, as for most container ships. For fast ships which have a very large transom stern, several researchers report problems. For submerged transom sterns at low speed, the potential flow model is inapplicable and only field methods are capable of an appropriate analysis.
- Kinematic condition: water does not penetrate the water surface.

- Dynamic condition: there is atmospheric pressure at the water surface. Beneath an air cushion, this condition modifies to the air cushion pressure. The inclusion of an air cushion in wave resistance computations has been reported in various applications. However, these computations require the user to specify the distribution of the pressure, especially the gradual decline of the pressure at the ends of the cushion. In reality, this is a difficult task as the dynamics of the air cushion and the flexible skirts make the problem more complicated. Subsequently, the computations must be expected to be less accurate than for conventional displacement hulls.
- Radiation condition: waves created by the ship do not propagate ahead. (This condition is not valid for shallow-water cases when the flow becomes unsteady and soliton waves are pulsed ahead. For subcritical speeds with depth Froude number $F_{nh} < 1$, this poses no problem.)
- Decay condition: the flow is undisturbed far away from the ship.
- Open-boundary condition: waves generated by the ship pass unreflected any artificial boundary of the computational domain.
- Equilibrium: the ship is in equilibrium, i.e. trim and sinkage are changed in such a way that the dynamical vertical force and the trim moment are counteracted.
- Bottom condition (shallow-water case): no water flows through the sea bottom.
- Side-wall condition (canal case): no water flows through the side walls.
- Kutta condition (for catamaran/SWATH): at the stern/end of the strut the flow separates. The Kutta condition describes a phenomenon associated with viscous effects. Potential flow methods use special techniques to ensure that the flow separates. However, the point of separation has to be determined externally 'by higher insight'. For geometries with sharp aftbodies (foils), this is quite simple. For twin-hull ships, the disturbance of the flow by one demi-hull induces a slightly non-uniform inflow at the other demi-hull. This resembles the flow around a foil at a very small angle of incidence. A simplified Kutta condition usually suffices to ensure a realistic flow pattern at the stern: zero transverse flow is enforced. This is sometimes called the 'Joukowski condition'.

The decay condition substitutes the open-boundary condition if the boundary of the computational domain lies at infinity. The decay condition also substitutes the bottom and side-wall conditions if bottom and side wall are at infinity, which is the usual case.

Hull, transom stern, and Kutta conditions are usually enforced numerically at collocation points. Also, a combination of kinematic and dynamic conditions is numerically fulfilled at collocation points. Combining dynamic and kinematic boundary conditions eliminates the unknown wave elevation, but yields a non-linear equation to be fulfilled at the a priori unknown free-surface elevation.

Classical methods linearize the differences between the actual flow and uniform flow to simplify the non-linear boundary condition to a linear condition fulfilled at the calm-water

surface. This condition is called the Kelvin condition. For practical applications, this crude approximation is unsuitable.

Dawson proposed in 1977 to use the potential of a double-body flow and the undisturbed water surface as a better approximation. Double-body linearization was popular until the early 1990s. The original boundary condition of Dawson was inconsistent. This inconsistency was copied by most subsequent publications following Dawson's approach. Sometimes this inconsistency is accepted deliberately to avoid evaluation of higher derivatives, but in most cases and possibly also in the original it was simply an oversight. Dawson's approach requires the evaluation of terms on the free surface along streamlines of the double-body flow. This required either more or less elaborate schemes for streamline tracking or some 'courage' in simply applying Dawson's approach on smooth grid lines on the free surface which were algebraically generated.

The first consistently linearized free-surface condition for arbitrary approximations of the base flow and the free-surface elevation was developed in Hamburg by Söding. This condition is rather complicated involving up to a third of the derivatives of the potential, but it can be simply repeated in an iterative process which is usually started with uniform flow and no waves.

Fully non-linear methods were first developed in Sweden and Germany in the late 1980s. The success of these methods quickly motivated various other research groups to copy the techniques and apply the methods commercially. The best-known codes used in commercial applications include SHIPFLOW-XPAN, SHALLO, ν-SHALLO, RAPID, SWIFT, and FSWAVE/VSAERO. The development is very near the limit of what potential flow codes can achieve. The state of the art is well documented in two PhD theses, Raven (1996) and Janson (1996). Despite occasional other claims, all 'fully non-linear' codes have similar capabilities when used by their designers or somebody well trained in using the specific code. Everybody loves his own child best, but objectively the differences are small. All 'fully non-linear' codes in commercial use share similar shortcomings when it comes to handling breaking waves, semi-planing or planing boats or extreme non-linearities. Free-surface RANSE methods are the appropriate tools in these cases where wave resistance codes are no longer applicable.

Waves propagate only downstream (except for rare shallow-water cases). This radiation condition has to be enforced by numerical techniques. Most methods employ special finite difference (FD) operators to compute second derivatives of the potential in the free-surface condition. Dawson proposed a four-point FD operator for second derivatives along streamlines. Beside the considered collocation point, the FD operator uses the next three points upstream. Dawson's method automatically requires grids oriented along streamlines of the double-body flow approximate solution. Dawson determined his operator by trial and error for a two-dimensional flow with a simple Kelvin condition. His criteria were that the wave length should

correspond to the analytically predicted wave length and the wave amplitude should remain constant some distance behind the disturbance causing the waves.

Dawson approximated the derivative of any function H with respect to ℓ at the point i numerically by:

$$H_{\ell i} \approx CA_i H_i + CB_i H_{i-1} + CC_i H_{i-2} + CD_i H_{i-3} \tag{3.81}$$

$H_{\ell i}$ is the derivative with respect to ℓ at point P_i. H_i to H_{i-3} are the values of the function H at points P_i to P_{i-3}, all lying on the same streamline of the double-body flow upstream of P_i. The coefficients CA_i to CD_i are determined from the arc lengths L_j ($j = 1$ to $i-3$) of the streamline between point P_i and point P_j:

$$L_j = \int_{P_i}^{P_j} \mathrm{d}\ell \quad \text{on the streamline} \tag{3.82}$$

$$CA_i = -(CB_i + CC_i + CD_i) \tag{3.83}$$

$$CB_i = L_{i-2}^2 L_{i-3}^2 (L_{i-3} - L_{i-2})(L_{i-3} + L_{i-2})/D_i \tag{3.84}$$

$$CC_i = -L_{i-1}^2 L_{i-3}^2 (L_{i-3} - L_{i-1})(L_{i-3} + L_{i-1})/D_i \tag{3.85}$$

$$CD_i = L_{i-1}^2 L_{i-2}^2 (L_{i-2} - L_{i-1})(L_{i-2} + L_{i-1})/D_i \tag{3.86}$$

$$D_i = L_{i-1} L_{i-2} L_{i-3} (L_{i-3} - L_{i-1})(L_{i-2} - L_{i-1})(L_{i-3} - L_{i-2}) \cdot (L_{i-3} + L_{i-2} + L_{i-1}) \tag{3.87}$$

This four-point FD operator dampens the waves to some extent and gives usual discretizations (about ten elements per wave length) wave lengths which are about 5% too short. Strong point-to-point oscillations of the source strength occur for very fine grids. Various FD operators have been subsequently investigated to overcome these disadvantages. Of all these, only the spline interpolation developed at MIT was really convincing as it overcomes all the problems of Dawson (Nakos 1990, Nakos and Sclavounos 1990).

An alternative approach to FD operators involves 'staggered grids' as developed in Hamburg. This technique adds an extra row of source points (or panels) at the downstream end of the computational domain and an extra row of collocation points at the upstream end (Fig. 3.12).

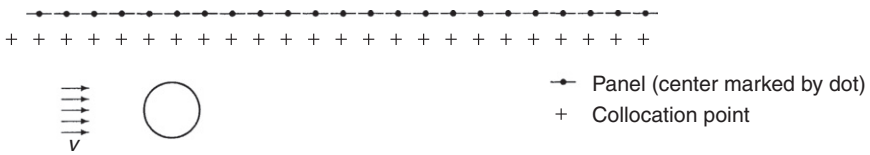

Figure 3.12:
'Shifting' technique (in 2d)

For equidistant grids this can also be interpreted as shifting or staggering the grid of collocation points vs. the grid of source elements. This technique shows absolutely no numerical damping or distortion of the wave length, but requires all derivatives in the formulation to be evaluated numerically.

Only part of the water surface can be discretized. This introduces an artificial boundary of the computational domain. Disturbances created at this artificial boundary can destroy the whole solution. Methods based on FD operators use simple two-point operators at the downstream end of the grid which strongly dampen waves. At the upstream end of the grid, where waves should not appear, various conditions can be used, e.g. the longitudinal component of the disturbance velocity is zero. Nakos (1990) has to ensure in his MIT method (SWAN code) based on spline interpolation that waves do not reach the side boundary. This leads to relatively broad computational domains. Time-domain versions of the SWAN code use a 'numerical beach'. For the wave resistance problem, the time-domain approach seems unnecessarily expensive and is rarely used in practice. Norwegian researchers tried to reduce the computational domain by matching the panel solution for the near-field to a thin-ship-theory solution in the far field. However, this approach saved only little computational time at the expense of a considerably more complicated code and was subsequently abandoned. The 'staggered grid' technique is again an elegant alternative. Without further special treatment, waves leave the computational domain without reflection.

Most methods integrate the pressure on the ship's surface to determine the forces (especially the resistance) and moments. 'Fully non-linear' methods integrate over the actually wetted surface while older methods often take the CWL as the upper boundary for the integration. An alternative to pressure integration is the analysis of the wave energy behind the ship (wave cut analysis). The wave resistance coefficients should theoretically tend to zero for low speeds. Pressure integration usually gives resistance coefficients which remain finite for small Froude numbers. However, wave cut analysis requires larger grids behind the ship, leading to increased computational time and storage. Most developers of wave resistance codes have at some point tried to incorporate wave cut analysis to determine the wave resistance more accurately. So far the evidence has not been compelling enough to abandon the direct pressure integration.

Most panel methods give as a direct result the source strengths of the panels. A subsequent computation determines the velocities at the individual points. Bernoulli's equation then gives pressures and wave elevations (again at individual points). Integration of pressures and wave heights finally yields the desired forces and moments, which in turn are used to determine dynamical trim and sinkage ('squat').

Fully non-linear state-of-the-art codes fulfill iteratively an equilibrium condition (dynamical trim and sinkage) and both kinematic and dynamic conditions on the actually deformed free surface. The differences in results between 'fully non-linear' and linear or 'somewhat non-linear' computations are considerable (typically 25%), but the agreement of computed and

measured resistances is not consistently better in 'fully non-linear' methods. This may in part be due to the computational procedure or inherent assumptions in computing a wave resistance from experimental data (usually using a form factor method), but also due to computational errors in determining the resistance, which are of similar magnitude as the actual resistance. One reason for the unsatisfactory accuracy of the numerical procedures lies in the numerical sensitivity of the pressure integration. The pressure integration basically involves subtracting forces of the same magnitude which largely cancel. The relative error is strongly propagated in such a case. Initial errors stem from the discretization. For example, integration of the hydrostatic pressure for the ship at rest should give zero longitudinal force, but usual discretizations show forces that may lie within the same order of magnitude as the wave resistance. Still, there is consensus that panel methods capture the pressure distribution at the bow quite accurately. The vertical force is not affected by the numerical sensitivity. Predictions for the dynamical sinkage usually differ by less than 5% for a large bandwidth of Froude numbers. Trim moment is not predicted as well due to viscous effects and numerical sensitivity. This tendency is amplified by shallow water.

Panel methods are still the most important CFD instrument for form improvement of ships. They are widely used by ship designers. For at least a decade, they have also been used in formal hull optimization in industrial applications. The fundamental limitation of panel methods lies in the neglect of viscosity (aftbody and appendages) and breaking waves. The intersection between water surface and ship will remain a problem zone for panel methods, because the problem is ill-posed here within a potential flow model. The immediate vicinity of the bow of a ship always features breaking waves and spray, which cannot be included by panel methods. Ad hoc solutions are subject to research, but no convincing solution has been published yet. In industry practice, these limitations are overcome by using free-surface RANSE methods rather than boundary element methods, when breaking waves must be captured. Free-surface RANSE methods can simulate flows with complicated free-surface geometries (breaking waves, splashes), allowing the analyses of problems beyond the realm of BEM applications.

3.5.2. Viscous Flow Computations

RANSE solvers are state of the art for viscous ship flows. A computational prediction of the total calm-water resistance using RANSE solvers to replace model tests would be desirable. So far the accuracy of the RANSE predictions is largely perceived as insufficient, but this is expected to change within the next decade. Nevertheless, RANSE solvers are widely applied to analyze:

- the flow around aftbodies of ships;
- the flow around appendages.

The first research applications for RANSE solutions with wave-making for ships appeared in the late 1980s. By the late 1990s various research groups also presented results for ships free to

trim and sink. Ten years later, free-surface RANSE computations were used regularly in many industry projects.

The basic techniques of RANSE codes have been discussed in Section 1.5. Various applications to ship design and research applications are found in the literature. Representative for the development of the state of the art for ship design applications are the proceedings of the Numerical Towing Tank Symposium (NuTTS) and surveys by leading companies in the field such as Flowtech (Larsson 1997, Larsson et al. 1998), or HSVA (Bertram and Jensen 1994, Bertram 1998a). The state of the art in research is documented in validation workshops like the Tokyo 1994 and 2005 workshops, the Gothenburg 2000 and 2010 workshops. RANSE computations require considerable skill and experience in grid generation and should therefore as a rule be executed by experts usually found in special consulting companies.

3.6. Simple Design Approaches

In early design stages, the power requirements have to be estimated to judge the weight and volume requirements of the main engine and fuel. As this has to be done repeatedly in design loops, model tests are not suitable solutions for reasons of time and costs. Instead, simple, largely empirical methods are employed which only require a few global design parameters. These methods are discussed in more detail by Schneekluth and Bertram (1998).

The main approaches are:

- Estimate from parent ship, e.g. by admiralty or similar formulae
  The estimate from a parent ship may give good estimates if the parent ship is close enough (in geometrical properties and speed parameters) to the design ship. The 'admiralty formula' is still used today, but only for a very rough estimate:

$$P_B = \frac{\Delta^{2/3} \cdot V^3}{C} \tag{3.88}$$

  The admiralty constant C is assumed to be constant for similar ships with similar Froude numbers, i.e. ships that have almost the same C_B, $C_B\ \nabla/L^3$, F_n, ∇, etc. Typical values for C [in $t^{2/3} \cdot kn^3 = kW$] are:

multi-purpose vessel	400−600
bulker and tanker	600−750
reefer	550−700
feeder ship	350−500
warship	150

  These values give an order of magnitude only. The constant C should be determined individually for basis ships used in design.

Generalized admiralty formulae are of the form:

$$P_B = \frac{\Delta^m \cdot V^n}{C} \tag{3.89}$$

where m and n are determined from regression analysis of databases.
Völker (1974) gives a modified admiralty formula for cargo ships with smaller scatter for C:

$$P_B = \frac{\Delta^{0.567} \cdot V^{3.6}}{C \cdot \eta_D} \tag{3.90}$$

η_D in this formula may be estimated by empirical formulae. Strictly speaking, the exponent of V should be a function of speed range and ship hull form. The admiralty formula is thus only useful if a ship of the same type, size, and speed range is selected to determine C. It is possible to increase the accuracy of the Völker formula by adjusting it to specific ship types.

The admiralty formula is very coarse and not recommended (unless a very close similar ship is used to determine C), but an estimate based on a form factor approach is popular in practice. Here, it is usually assumed that the parameter c_w/F_n^4 and the form factor remain constant in the conversion from parent ship to design ship. Such a more or less sophisticated plus/minus conversion from a parent ship is currently the preferred choice for a quick estimate.

Tugs are special ships which differ in many ways from regular cargo ships (Allan 2004). The main design specification concerns maneuverability and ability to assist escort vessels in maneuvering. This requires a somewhat different approach in design. Bertram and Bentin (2001) use neural nets to express the required power P_B [kW] of harbor tugs as function of design speed V [kn], bollard pull b_p [t] and length between perpendiculars L_{pp} [m]:

$$\begin{aligned} P_B = 1060 + 3354 \cdot \mathrm{sig}(1.23 - 6.44 \cdot \mathrm{sig}(0.08652 \cdot L_{pp} - 0.3171 \cdot\ b_p - 3.84 \cdot V \\ + 60.4709) + 2.97 \cdot \mathrm{sig}(0.8539 \cdot L_{pp} + 0.2307 \cdot\ b_p - 0.484 \cdot V \\ - 23.07) - 5.98 \cdot \mathrm{sig}(0.2596 \cdot L_{pp} + 0.0856 \cdot\ b_p + 0.51 \cdot V \\ - 17.577) + 2.61 \cdot \mathrm{sig}(0.2857 \cdot L_{pp} + 0.7132 \cdot\ b_p + 0.476 \cdot V \\ - 25.7645)) \end{aligned} \tag{3.91}$$

- Systematic series (e.g. Taylor−Gertler, Series-60, SSPA) or regression analysis of many ships (e.g. Lap−Keller, Holtrop−Mennen, Hollenbach)
  All of the systematic series and most of the regression analysis approaches are outdated. They often underestimate the actual resistance of modern ship hulls. It may come as a surprise that older ships were apparently better in terms of resistance. There are several explanations:
  - suitability for container stowage plays a larger role in modern ships;
  - modern ships often have a higher propulsive efficiency compensating partially for the higher resistance;

- more severe safety regulations, e.g. concerning stability, pose additional constraints on the hydrodynamic optimization.

It is fairly difficult to estimate accurately the residual resistance or the wave resistance. The method of choice today would be a CFD code, but for a quick estimate one may accept larger margins of errors and resort to classical estimates. Schneekluth and Bertram (1998) list some of the older methods for resistance predictions including the Lap−Keller method. These methods are historical and should no longer be applied in modern ship design. More 'modern' methods which are often found imbedded in ship design systems are (Table 3.2):

- 'Taylor−Gertler' (for slender ships) (Gertler 1954)
- 'Guldhammer−Harvald' (Guldhammer and Harvald 1974)
- 'Holtrop−Mennen' (Holtrop and Mennen 1978, 1982, Holtrop 1977, 1978, 1984)
- 'Hollenbach' (Hollenbach 1998, 1999)
- 'NPL' (for fast ships) (Bailey 1976).

The older methods like 'Taylor−Gertler' do not consider the bulbous bow. The effect of a bulbous bow may then be approximately introduced by increasing the length in the calculation by two-thirds of the bulb length.

Oortmerssen (1971) presents a simple method to estimate the residual resistance of tugs and trawlers based on regression analysis of model basin data. The range of parameters for which the coefficients of the basic expressions are valid, are as follows: $8\,\text{m} < L_{WL} < 80\,\text{m}$; $5\,\text{m}^3 < \nabla < 3000\,\text{m}^3$; $3 < L/B < 6.2$; $1.9 < B/T < 4.0$; $0.50 < C_P < 0.73$; $0.70 < C_M < 0.97$; $-7\%\ L < lcb < 2.8\%\ L$ forward of $0.5\ L$; $0 < F_n < 0.5$; $10^\circ < i_E < 46^\circ$. i_E is the half angle of entrance of the design waterline. The residual resistance made non-dimensional by the displacement weight in his expression:

$$\frac{R_R}{\Delta \cdot g} = C_1 \cdot \exp\left(-\frac{mF_n^2}{9}\right) + C_2 \cdot \exp\left(-\frac{m}{F_n^2}\right) + C_3 \cdot \exp\left(-mF_n^2\right) \cdot \sin\left(\frac{1}{F_n^2}\right) + C_4 \cdot \exp(-mF_n^2) \cdot \cos\left(\frac{1}{F_n^2}\right) \tag{3.92}$$

$$\begin{aligned} C_1 \cdot 10^3 = {} & 79.32134 - 0.09287\ lcb - 0.00209\ lcb^2 - 246.45896\ C_P + 187.13664\ C_P^2 \\ & -1.42893\ L/B + 0.11898\ (L/B)^2 + 0.15727\ C_{IE} - 0.00064\ C_{IE}^2 \\ & -2.52862\ B/T + 0.50619\ (B/T)^2 + 1.62851\ C_M \end{aligned} \tag{3.93}$$

$$\begin{aligned} C_2 \cdot 10^3 = {} & 6714.88397 + 19.83\ lcb + 2.66997\ lcb^2 - 19662.024\ C_P + 14099.9\ C_P^2 \\ & +137.33613\ L/B - 13.36938\ (L/B)^2 - 4.49852\ C_{IE} + 0.021\ C_{IE}^2 \\ & +216.44923\ B/T - 35.07602\ (B/T)^2 - 128.72535\ C_M \end{aligned} \tag{3.94}$$

$$\begin{aligned} C_3 \cdot 10^3 = {} & -908.44371 + 2.52704\ lcb - 0.35794\ lcb^2 + 755.1866\ C_P - 48.93952\ C_P^2 \\ & + 9.86873\ L/B\ -\ 0.77652\ (L/B)2\ +\ 3.79020\ C_{IE}\ -\ 0.01879\ C_{IE}^2 \\ & -9.24399\ B/T + 1.28571\ (B/T)^2 + 250.6491\ C_M \end{aligned} \tag{3.95}$$

Table 3.2: Resistance prediction methods

Resistance procedure 'Taylor–Gertler'
Basis for procedure: Systematic model tests with a model warship *Target value:* C_R *Input values:* L_{wl}; $F_{n,wl} = V/\sqrt{g \cdot L_{wl}}$; $C_{P,wl} = \nabla/L_{wl}^3$; B/T; S *Remarks:* 1. Influence of bulb not taken into account 2. The procedure generally underestimates by 5–10% 3. Area of application: fast cargo ships, warships 4. Constant or dependent variable values: $C_M = 0.925 = \text{constant}$, $lcb = 0.5\ L_{wl}$
Resistance procedure 'Guldhammer–Harvald'
Basis for procedure: Evaluation of well-known resistance calculation procedures (Taylor, Lap, Series 60, Gothenburg, BSRA, etc.) *Target value:* C_R and C_F *Input values:* L_{wl}; $F_{n,wl}$; B/T; lcb, section shape; A_{BT} (bulb); S; $C_{P,wl}$; $L_{wl}/\nabla^{1/3}$ *Remarks:* 1. Influence of bulb taken into account 2. Reference to length in WL 3. Area of application: universal, tankers 4. The correction for the center of buoyancy appears (from area to area) overestimated 5. The procedure underestimates resistance for ships with small L/B
Resistance procedure 'Holtrop–Mennen'
Basis for procedure: Evaluation of database of the Dutch Model Basin MARIN *Target value:* C_T *Input values:* F_n; L_{pp}; L_{wl}; B; T; ∇; lcb; C_{WP}; S; section shape; trim; … *Remarks:* 1. Resistance decomposition like ITTC'78 2. Considers bulbous bow and transom stern 3. Covers wide range of ships 4. Many parameters; some may have to be estimated in early design
Resistance procedure 'Hollenbach'
Basis for procedure: Evaluation of database of Vienna ship model basin *Target value:* R_T *Input values:* F_n; L_{pp}; L_{wl}; B; T; C_B; D_P; trim; number of appendages *Remarks:* 1. Considers twin-screw ships 2. Relatively modern database 3. Applicable to modern cargo ship 4. Several typing mistakes between various publications 5. Gives also 'minimum' and 'maximum' resistance curves
Resistance procedure 'NPL Series'
Basis for procedure: Systematic model tests with high-speed, round-bilge displacement forms *Target value:* $R_R/(\nabla \cdot g)$

Table 3.2: Continued

Input values: $F_{n\nabla}$; L/B; $L/\nabla^{1/3}$ *Remarks:* 1. For fast displacement ships; (originally) graphical method 2. Simple HSVA formulae recommended instead as easy to program and based on more modern ship designs
Resistance procedure 'Van Oortmerssen'
Basis for procedure: Evaluation of database of Dutch model basin MARIN for small ships *Target value:* $R_R/(\nabla \cdot g)$ *Input values:* F_n; lcb, L/B; B/T; C_M; C_{IE}; C_P; $L/\nabla^{1/3}$ *Remarks:* 1. For tugs and trawlers up to $F_n = 0.5$ 2. $C_{IE} = i_E \cdot L/B$, where i_E is the half angle of entrance of the design waterline 3. Easy to program

$$\begin{aligned} C^4 \cdot 10^3 &= 3012.14549 + 2.71437\ lcb + 0.25521\ lcb^2 - 9198.8084\ C_P \\ &+6886.60416\ C_P^2 - 159.92694\ L/B + 16.23621\ (L/B)^2 - 0.82014\ C_{IE} \\ &+0.00225\ C_{IE}^2 + 236.3797\ B/T - 44.1782\ (B/T)^2 + 207.2558\ C_M \end{aligned} \tag{3.96}$$

$$m = 0.14347\ C_P^{-2.1976} \tag{3.97}$$

$C_{IE} = i_E \cdot L/B$, where i_E is taken in degrees. $L = (L_{PP}+L_{WL})/2$ in Van Oortmerssen's formula.

MacPherson (1993) provides some background and guidance to designers for simple computer-based prediction methods, and these are recommended for further studies.

Some of the old estimation methods are still popular as they are easy to program. Thus they are embedded in naval architectural CAD systems or more recently in design expert systems. However, they are fundamentally limited to global predictions, as they represent the hull shape by few global parameters.

The following compiles assorted simple design formulae, mostly taken from Schneekluth and Bertram (1998):

- Propulsive efficiency η_D
  Typical values are: $\eta_D \approx 0.6{-}0.7$ for cargo ships
  $\eta_D \approx 0.4{-}0.6$ for tugs
  Danckwardt (1969) gives the following estimate (Henschke 1965):

$$\eta_D = 0.836 - 0.000165 \cdot n \cdot \nabla^{1/6} \tag{3.98}$$

n is the propeller rpm and ∇ [m^3] the displacement volume. All ships checked were within $\pm 10\%$ of this estimate; half of the ships were within $\pm 2.5\%$.

Keller (1973) gives:

$$\eta_D = 0.885 - 0.00012 \cdot n \cdot \sqrt{L_{pp}} \tag{3.99}$$

HSVA gave, for twin-screw ships, in 1957:

$$\eta_D = 0.69 - 12000 \cdot \left(0.041 - \frac{V_s}{n \cdot D_p}\right)^3 \pm 0.02 \tag{3.100}$$

Ship speed V_s [in kn], propeller diameter D_p [in m], $0.016 \leq V_s/(n \cdot D_p) \leq 0.04$.

- Hull efficiency η_H

  The hull efficiency can be estimated indirectly by estimating thrust deduction fraction t and wake fraction w separately or directly. For small ships with rake of keel, Helm (1980) gives an empirical formula:

$$\eta_H = 0.895 - \frac{0.0065 \cdot L}{\nabla^{1/3}} - 0.005 \cdot \frac{B}{T} - 0.033 \cdot C_P + 0.2 \cdot C_M + 0.01 \cdot lcb \tag{3.101}$$

  lcb here is the longitudinal center of buoyancy taken from $L_{pp}/2$ [in $\%L_{pp}$]. The basis for this formula covers $3.5 \leq L/\nabla^{1/3} \leq 5.5$, $0.53 \leq C_P \leq 0.71$, $2.25 \leq B/T \leq 4.50$, $0.60 \leq C_M \leq 0.89$, rake of keel $40\%T$, $D_P = 0.75T$. T is taken amidships.

  Usually, it is preferable to estimate t and w separately and then deduct η_H from there.

- Thrust deduction fraction t

  For single-screw ships:

$$t = 0.5 \cdot C_P - 0.12; \quad \text{Heckscher for cargo ships} \tag{3.102}$$

$$t = 0.77 \cdot C_P - 0.30; \quad \text{Heckscher for trawlers} \tag{3.103}$$

$$t = 0.5 \cdot C_B - 0.15; \quad \text{Danckwardt for cargo ships} \tag{3.104}$$

$$t = w \cdot (1.57 - 2.3 \cdot C_B/C_{WP} + 1.5 \cdot C_B); \quad \text{SSPA for cargo ships} \tag{3.105}$$

$$t = 0.001979 \cdot \frac{L}{B(1 - C_P)} + 1.0585 \cdot \frac{B}{L} - 0.00524 - 0.1418 \cdot \frac{D_P^2}{BT}; \quad \text{Holtrop and Mennen} \tag{3.106}$$

  For twin-screw ships:

$$t = 0.5 \cdot C_P - 0.18; \quad \text{Heckscher for cargo ships} \tag{3.107}$$

$$t = 0.52 \cdot C_B - 0.18; \quad \text{Danckwardt for cargo ships} \tag{3.108}$$

$$t = w \cdot (1.67 - 2.3 \cdot C_B/C_{WP} + 1.5 \cdot C_B); \quad \text{SSPA for cargo ships} \tag{3.109}$$

$$t = 0.325 \cdot C_B - 0.1885 \cdot \frac{D_P}{\sqrt{BT}}; \quad \text{Holtrop and Mennen} \tag{3.110}$$

Alte and Baur (1986) give an empirical coupling between t and the wake fraction w:

$$(1 - t) = (1 - w)^{0.4-0.8} \tag{3.111}$$

In general, in the early design stage it cannot be determined which t will give the best hull efficiency η_H. t can be estimated only roughly in the design stage and all of the above formulae have a much larger uncertainty margin than those for w given below. t thus represents the largest uncertainty factor in the power prognosis.

- Wake fraction w

For single-screw ships:

$$w = 0.5 \cdot C_P \cdot \frac{1.6}{1 + D_P/T} \cdot \frac{16}{10 + L/B}; \quad \text{Schneekluth for ships with stern bulb} \tag{3.112}$$

$$w = 0.75 \cdot C_B - 0.24; \quad \text{Krüger} \tag{3.113}$$

$$w = 0.7 \cdot C_P - 0.18; \quad \text{Heckscher for cargo ships} \tag{3.114}$$

$$w = 0.77 \cdot C_P - 0.28; \quad \text{Heckscher for trawlers} \tag{3.115}$$

$$w = 0.25 + 2.5(C_B - 0.6)^2; \quad \text{Troost for cargo ships} \tag{3.116}$$

$$w = 0.5 \cdot C_B; \quad \text{Troost for coastal feeders} \tag{3.117}$$

$$w = C_B/3 + 0.01; \quad \text{Caldwell for tugs with } 0.47 < C_B < 0.56 \tag{3.118}$$

$$w = 0.165 \cdot C_B \cdot \frac{\nabla^{1/3}}{D_P} - 0.1 \cdot (F_n - 0.2); \quad \text{Papmehl} \tag{3.119}$$

$$w = \frac{3}{1 - (C_P/C_{WP})^2} \cdot \frac{B}{L} \cdot \frac{E}{T} \cdot \left[1 - \frac{1.5 \cdot D + (\varepsilon + r)}{B}\right]; \quad \text{Telfer for cargo ships} \tag{3.120}$$

ε is the skew angle in radians, r is the rake angle in radians, and E is height of the shaft center over keel.

For twin-screw ships:

$$w = 0.81 \cdot C_B - 0.34; \quad \text{Krüger} \tag{3.121}$$

$$w = 0.7 \cdot C_P - 0.3; \quad \text{Heckscher for cargo ships} \tag{3.122}$$

$$w = C_B/3 - 0.03; \quad \text{Caldwell for tugs with } 0.47 < C_B < 0.56 \tag{3.123}$$

Holtrop and Mennen (1978) and Holtrop (1984) give further more complicated formulae for w for single-screw and twin-screw ships, which can be integrated in a power prognosis program.

All the above formulae consider only a few main parameters, but the shape of the ship, especially the aftbody, influences the wake considerably. Other important parameters are propeller diameter and propeller clearance, which are not explicitly represented in the above formulae. For bulk carriers with $C_B \approx 0{:}85$, $w < 0.3$ have been obtained by form optimization. The above formulae can thus predict too high w values for full ships.

- Relative rotative efficiency η_R

  The relative rotative efficiency is driven by many different effects. This makes it difficult to express η_R as a function of just a few parameters.
  Holtrop and Mennen (1978) and Holtrop (1984) give:

$$\eta_R = 0.9922 - 0.05908 \cdot A_E/A_0 + 0.07424 \cdot (C_P - 0.0225 \cdot lcb) \quad \text{for single-screw ships} \tag{3.124}$$

$$\eta_R = 0.9737 - 0.111 \cdot (C_P - 0.0225 \cdot lcb) - 0.06325 \cdot P/D_P \quad \text{for twin-screw ships} \tag{3.125}$$

  lcb here is the longitudinal center of buoyancy taken from $L_{wl}/2$ [in $\%L_{wl}$]
  A_E/A_0 is the blade area ratio of the propeller
  P/D_P is the pitch-to-diameter ratio of the propeller.
  Helm (1980) gives for small ships:

$$\eta_R = 0.826 + 0.01\frac{L}{\nabla^{1/3}} + 0.02\,\frac{B}{T} + 0.1 \cdot C_M \tag{3.126}$$

  The basis for this formula is the same as for Helm's formula for η_H.
  Alte and Baur (1986) recommend, as a simple estimate, $\eta_R = 1.00$ for single-screw ships, $\eta_R = 0.98$ for twin-screw ships.
  Jensen (1994) gives $\eta_R = 1.02{-}1.06$ for single-screw ships, depending also on details of the experimental and correlation procedure.

- Wetted surface S

  Non-dimensional resistance coefficients require the wetted surface S, usually taken at calm-water conditions. CAD systems compute S accurately, but if only the main dimensions are known, one may resort to estimates:

$$S = \nabla^{1/3} \cdot (3.4 \cdot \nabla^{1/3} + 0.5 \cdot L_{wl}) \quad \text{Lap (1954) for cargo ships and ferries} \tag{3.127}$$

$$S = L \cdot (1.8 \cdot T + C_B \cdot B) \quad \text{Schneekluth for warships} \tag{3.128}$$

$$S = \frac{\nabla}{B} \cdot \left[\frac{1.7}{C_B - 0.2 \cdot (C_B - 0.65)} + \frac{B}{T}\right] \quad \text{Danckwardt for cargo ships and ferries} \tag{3.129}$$

$$S = \frac{\nabla}{B} \cdot \left[\frac{1.7}{C_B} + \frac{B}{T} \cdot (0.92 + \frac{0.092}{C_B})\right] \quad \text{Danckwardt for trawlers} \tag{3.130}$$

$$S = L \cdot (2T + B) \cdot C_M^{0.5} \cdot (0.453 + 0.4425 \cdot C_B - 0.2862 \cdot C_M - 0.003467 \cdot B/T + 0.3696 \cdot C_{WP}) \quad \text{Holtrop–Mennen for cargo ships} \tag{3.131}$$

- Viscous pressure resistance coefficient C_{PV}

$$C_{PV} \cdot 10^3 = (26 \cdot C_\nabla + 0.16) + \left(\frac{B}{T} - \frac{13 - 10^3 \cdot C_\nabla}{6}\right) \cdot (C_P + 58 \cdot C_\nabla - 0.408) \cdot (0.535 - 35 \cdot C_\nabla) \tag{3.132}$$

The formula was derived by Schneekluth from the Taylor experiments (dating back to 1910 and 1954), based on $B/T = 2.25–4.5$, $C_P = 0.48–0.8$, $C_\nabla = \nabla/L^3 = 0.001–0.007$.

- Form factor $k = R_{PV}/R_F$

$$k = 18.7 \cdot (C_B \cdot B/L)^2 \quad \text{Granville (1956)} \tag{3.133}$$

$$k = 14 \cdot (\nabla/L^3) \cdot (B/T) \quad \text{Alte and Baur (1986)} \tag{3.134}$$

$$k = -0.095 + 25.6 \cdot \frac{C_B}{(L/B)^2 \cdot \sqrt{B/T}} \quad \text{Watanabe (1986)} \tag{3.135}$$

- Appendage resistance R_{APP}

Simple semi-empirical formula for appendages are:

Exposed shafting, stern tubes and bossings:

$$R_{APP} = \frac{1}{2} \rho V^2 Ld (1.1 \sin^3 \varepsilon + \pi C_F) \tag{3.136}$$

Here C_F is calculated with a Reynolds number based on the diameter d. L is the length of shaft and ε its inclination relative to the keel.

Struts and rudders:

$$R_{APP} = \rho V^2 S C_F (1 + 2(t/c) + 60(t/c)^4) \tag{3.137}$$

Here C_F is calculated with a Reynolds number based on chord length c. t is the thickness of the strut and S the projected surface (one side) of the strut.

Bilge keels:

$$R_{APP} = \rho V^2 S_B C_F \tag{3.138}$$

Here C_F is calculated with a Reynolds number based on the bilge keel length.
Transom wedges:

$$R_{APP} = 0.0001196\, c\, \delta\, \rho\, V^2\, S(\tau + \delta) \tag{3.139}$$

Here δ is the wedge angle, τ the trim angle of the vessel (positive stern down), S the wetted surface, and c the chord length of the wedge.

- Wind resistance R_{AA}
  Wind resistance is important for ships with large lateral areas above the water level, e.g. container ships and car ferries. Fast and unconventional ships, e.g. air-cushioned vehicles, also require inclusion of the contribution of wind or air resistance. Jensen (1994) gives a very simple estimate for the wind resistance of cargo ships:

$$R_{AA} = C_{AA} \cdot \frac{\rho_{\text{air}}}{2} \cdot (V + V_{\text{wind}})^2 \cdot A_F \tag{3.140}$$

For cargo ships, Jensen (1994) gives $C_{AA} = 0.8{-}1.0$. $\rho_{\text{air}} = 1.25\ \text{kg/m}^3$ the density of air, V_{wind} is the absolute value of wind speed and A_F is the frontal projected area of the ship above sea level.
The wind resistance may be estimated with more accuracy following Blendermann (1993, 1996):

$$R_{AA} = \frac{\rho_{\text{air}}}{2} \cdot u^2 \cdot A_L \cdot CD_l \cdot \frac{\cos \varepsilon}{1 - \frac{\delta}{2}\left(1 - \frac{CD_l}{CD_t}\right)\sin^2 2\varepsilon} \tag{3.141}$$

Here u is the apparent wind velocity, A_L the lateral-plane area, ε the apparent wind angle ($\varepsilon = 0^\circ$ in head wind), and δ the cross-force parameter. CD_t and CD_l are the non-dimensional drag coefficients in beam wind and head wind, respectively. It is convenient to give the longitudinal drag with respect to the frontal projected area A_F:

$$CD_{l,AF} = CD_l \cdot \frac{A_L}{A_F} \tag{3.142}$$

Table 3.3 gives typical values for CD_t, $CD_{l,AF}$ and δ. The maximum wind resistance usually occurs for $0^\circ < \varepsilon < 20^\circ$. The above formulae and the values in the table are for uniform or nearly uniform flow, e.g. above the ocean. The wind speed at a height of 10 m above sea level u_{10} is usually taken as reference speed. Wind speed in Beaufort (Beaufort number BN) is converted to m/s by:

$$u_{10} = 0.836 \cdot BN^{1.5} \tag{3.143}$$

- Speed loss in wind and waves

Table 3.3: Coefficients to estimate wind resistance (Blendermann 1996)

	CD_t	$CD_{l,AF}$	δ
Car carrier	0.95	0.55	0.80
Cargo ship, container on deck, bridge aft	0.85	0.65/0.55	0.40
Containership, loaded	0.90	0.55	0.40
Destroyer	0.85	0.60	0.65
Diving support vessel	0.90	0.60	0.55
Drilling vessel	1.00	0.70−1.00	0.10
Ferry	0.90	0.45	0.80
Fishing vessel	0.95	0.70	0.40
LNG tanker	0.70	0.60	0.50
Offshore supply vessel	0.90	0.55	0.55
Passenger liner	0.90	0.40	0.80
Research vessel	0.85	0.55	0.60
Speedboat	0.90	0.55	0.60
Tanker, loaded	0.70	0.90	0.40
Tanker, in ballast	0.70	0.75	0.40
Tender	0.85	0.55	0.65

Townsin and Kwon (1983) give simple approximate formulae to estimate the speed loss due to added resistance in wind and waves:

$$\Delta V = C_\mu \cdot C_{\text{ship}} \cdot V\% \tag{3.144}$$

C_μ is a factor considering the predominant direction of wind and waves, depending on the Beaufort number BN:

$$C_\mu = 1.0 \quad \text{for } \mu = 0{-}30^\circ \tag{3.145}$$

$$C_\mu = 1.7 - 0.03 \cdot (BN - 4)^2 \quad \text{for } \mu = 30{-}60^\circ \tag{3.146}$$

$$C_\mu = 0.9 - 0.06 \cdot (BN - 6)^2 \quad \text{for } \mu = 60{-}150^\circ \tag{3.147}$$

$$C_\mu = 0.4 - 0.03 \cdot (BN - 8)^2 \quad \text{for } \mu = 150{-}180^\circ \tag{3.148}$$

C_{ship} is a factor considering the ship type:

$$C_{\text{ship}} = 0.5BN + BN^{6.5}/(2.7 \cdot \nabla^{2/3}) \quad \text{for tankers, laden} \tag{3.149}$$

$$C_{\text{ship}} = 0.7BN + BN^{6.5}/(2.7 \cdot \nabla^{2/3}) \quad \text{for tankers, ballast} \tag{3.150}$$

$$C_{\text{ship}} = 0.7BN + BN^{6.5}/(2.2 \cdot \nabla^{2/3}) \quad \text{for container ships} \tag{3.151}$$

∇ is the volume displacement in m^3. Tables 3.4 and 3.5 give relations between Beaufort number, wind speeds, and average wave heights.

Table 3.4: Wind strengths in Beaufort (Bft) (Henschke 1965)

Bft	Wind description	Wind speed
0	No wind	0.0–0.2 m/s
1	Gentle current of air	0.3–1.5 m/s
2	Gentle breeze	1.6–3.3 m/s
3	Light breeze	3.4–5.4 m/s
4	Moderate breeze	5.5–7.9 m/s
5	Fresh breeze	8.0–10.7 m/s
6	Strong wind	10.8–13.8 m/s
7	Stiff wind	13.9–17.1 m/s
8	Violent wind	17.2–20.7 m/s
9	Storm	20.8–24.4 m/s
10	Violent storm	24.5–28.3 m/s
11	Hurricane-like storm	28.5–32.7 m/s
12	Hurricane	>32.7 m/s

Table 3.5: Sea strengths for North Sea coupled to wind strengths (Henschke 1965)

			Approximate average	
Sea state	Bft	Sea description	Wave height	Wave length
0	0	Smooth sea	–	–
1	1	Calm, rippling sea	0–0.5 m	0–10 m
2	2–3	Gentle sea	0.5–0.75 m	10–12.5 m
3	4	Light sea	0.75–1.25 m	12.5–22.5 m
4	5	Moderate sea	1.25–2.0 m	22.5–37.5 m
5	6	Rough sea	2.0–3.5 m	37.5–60.0 m
6	7	Very rough sea	3.5–6.0 m	60.0–105.0 m
7	8–9	High sea	>6.0 m	>105.0 m
8	10	Very high sea	Up to 20 m	Up to 600 m
9	11–12	Extremely heavy sea	Up to 20 m	Up to 600 m

- Natural periods for ship motions
  For 'normal' ships, the natural frequencies in roll, heave, and pitch can be estimated by simple formulae.
  Natural roll period [s]:

$$T_{\text{roll}} = C \cdot \frac{B}{\sqrt{GM}} \tag{3.152}$$

with

$$C = 0.746 + 0.046\frac{B}{T} - 0.086 \cdot \frac{L}{100} \quad \text{following IMO} \tag{3.153}$$

$C = 0.7627–0.8229$ (typically 0.8) for cargo ships following Parsons (2004)

$C = 0.6924-1.0035$ generally following Parsons (2004)
B [m] is the width, L [m] the length in the waterline, T [m] the draft, GM [m] the metacentric height.
Natural pitch period [s]:

$$T_{\text{pitch}} = C \cdot \frac{L}{\sqrt{GM_L}} \tag{3.154}$$

$C = 0.4817-0.5218$ generally following Parsons (2004)
L [m] is the length in the waterline.

$$T_{\text{pitch}} = 1.776 \cdot \frac{\sqrt{TC_B(0.6 + 0.36 \cdot B/T)}}{C_{WP}} \quad \text{following Lamb (1969)} \tag{3.155}$$

B [m] is the width, T [m] the draft, C_B the block coefficient, and C_{WP} the waterplane coefficient.
Natural heave period [s]:

$$T_{\text{heave}} = 2.007 \cdot \sqrt{T\frac{C_B}{C_{WP}} \cdot \left(\frac{B}{3T} + 1.2\right)} \quad \text{following Lamb (1969)} \tag{3.156}$$

Variables as above for pitch period.

3.7. Fuel-Saving Options

3.7.1. Introduction

For decades, ships have been designed for much lower fuel costs. Increasing fuel prices and IMO regulations to curb CO_2 (carbon dioxide) emissions put pressure on ship owners to obtain more fuel-efficient ships. As a result, we have seen a renaissance of some concepts of the 1970s which were developed in response to the first oil crisis, as well as new proposals for fuel-saving devices. Many publications (including promotional material by companies) give unrealistically optimistic claims for fuel-saving potential of these devices. There are various reasons for false estimations:

- The published savings achieved with a particular device are normally for the best case. For example, formal hull optimization has improved the fuel efficiency of one vessel by 16% at design speed and draft. Subsequent literature then – correctly – states that up to 16% may be gained. This is quoted as '16% gains' in a subsequent survey or report and taken as typical value.

- Quoted savings are valid for initially bad designs, whereas hydrodynamically optimized designs would never reach that saving.
- Numbers valid for one certain ship type (say high-speed container vessels) are taken for other ships (e.g. bulk carriers), where they do not apply.
- Numbers are taken for design speed and draft. Frequently encountered off-design conditions are ignored. Utilization of a fuel-saving device is often incorrectly assumed to be 100% of the time at sea for a ship and 100% over fleets for global estimates.
- Saving potential refers to calm-water resistance, but is applied to total resistance or total fuel consumption (including the on-board energy consumption).
- For propulsion-improving devices, published savings are based on a comparison of power requirement measured before and after conversion. Measurements are not corrected for hull and propeller roughness (ship and propeller are often cleaned while the ship is refitted with a propulsion-improving device), sea state and loading condition. If measures are corrected for a 'neutral condition', the correction procedure in itself has an uncertainty of 2−3%.
- Saving potential is quoted based on model tests and questionable extrapolation to full scale. Model tests violate Reynolds similarity and hence boundary layers and flows at appendages in the boundary layer are not similar. Most quoted figures are based on publications (and model tests) of the 1970s and 1980s. There is usually no documentation on how figures were derived. In my personal experience, re-analyses and detailed full-scale measurements with today's technology always showed substantially lower figures.

3.7.2. Global Measures to Reduce Resistance

On the most global level, there are two (almost trivial) options following from the admiralty formula:

- Reduce ship size. The ship size (or displacement) is driven by the cargo weight, ballast, steel weight and equipment, and outfit weight. The fuel consumption scales with displacement to the power 2/3. As cargo weight usually is a fixed quantity and dominates the overall displacement, savings through minimizing steel weight and ballast are usually only small to moderate. However, other measures to reduce power requirements lead to smaller engines and associated periphery (power trains, cooling pumps, fuel tanks, etc.). This yields secondary savings in new designs due to smaller ship size.
- Reduce speed. Speed reduction is a very effective way to reduce fuel consumption and emission. The admiralty formula assumes a cubic relationship between power and speed. This is a widely used assumption for small speed changes, but actual speed curves exhibit local deviations from this rule of thumb. The rule applies for the bare-hull, calm-water condition. A 10% speed reduction (i.e. taking 90% of the reference speed) yields a 27% reduction in required power ($0.9^3 = 0.73$). In addition, slower design speeds allow higher propeller efficiency. This may add another 2% fuel savings for 10% design speed

reduction. Slower speed often also results in lower added resistance in seaways. As mentioned above, there are secondary savings to the smaller installed engine power. For new buildings, design for slower speed is thus a very effective lever to reduce fuel consumption. Necessary measures to keep delivery capacity constant (larger fleet size or larger cargo capacity) may increase fuel consumption in fleets by 6−8% (as port times are not affected by ship speed). The net reduction in fuel consumption is then 23−25% for 10% design speed reduction and constant delivery capacity. Several factors introduce penalties or constraints for lower speeds:

- Lower speed often attracts less cargo.
- Capital costs of cargo depend on transport time and cargo value. Slower transport increases capital costs on the cargo and reduces freight rates accordingly.
- Transitional costs for logistics pose barriers in intermodal transport chains. These costs occur once for adapting existing schedules, but can be considerable in large transport networks.
- Slower ships transport less and additional ships are needed to maintain a transport capacity. Correspondingly, crew costs increase.
- The auxiliary power needed for crew (hotel-load), navigation and (if applicable) cargo care is independent of speed. Correspondingly, the associated costs increase.
- Safety aspects pose lower limits for very low speeds. However, a 10% reduction in design speed is generally not critical in this respect.

Reduced speed for existing ships is called slow steaming. Slow steaming is less effective than designing for lower speed as there are no savings for better propeller efficiency and lower ship weight. Instead, hull, propeller, and engine operate in an off-design condition and thus at a lower efficiency. Slow steaming is adopted only when there is a slump in demand for shipping transport. Extended operation in off-design conditions leads to increased maintenance and down-time costs. In addition to technical obstacles, non-technical obstacles (like existing delivery contracts and logistics chains) hinder wider adoption.

In the following, we consider more detailed options for given speed and displacement. The attractiveness or sense of these measures depends generally on the composition of the total resistance of a ship, which differs significantly between various ship types. It is recommended to estimate at the beginning of a project the composition of the total resistance to facilitate a subsequent discussion on the effectiveness of fuel-saving measures.

Ships experience added resistance in seaways. This resistance is dominated in long waves by the ship motions, in short waves by wave reflection/diffraction. The motions can be influenced mainly by the length of the ship and to some extent by local shape details (flare of foreship or X-bow for example). The added resistance in seaways (and the saving potential for this item) is generally larger for smaller ships. For large ships, the reflection/diffraction can be reduced by different bow forms. Such proposals appear to be academic and not attractive in a holistic view.

Ideally, total power requirements should be minimized, considering also added resistance in waves in design (or even formal optimization). This has been proposed, but requires reliable prediction of the added resistance in waves. Added resistance in waves is difficult to measure and compute. Options to reduce added resistance in seaways by routing are discussed further below.

3.7.3. Hull Coatings and Air Lubrication

The frictional resistance is generally the largest part of the total resistance. The frictional resistance (for a given speed) is governed by wetted surface (main dimensions and trim) and surface roughness of the hull (average hull roughness of coating, added roughness due to fouling and coating degradation). Ships with severe fouling may require twice the power as with a smooth surface. Munk (2006) estimates that only one-third of the world fleet is in good coating condition with less than 20% added resistance compared to smooth surface condition.

Advanced hull coatings can reduce frictional resistance. An average hull roughness (AHR) of 65 μm is very good, 150 μm standard, and AHR $>$ 200 μm sub-standard. As a rule of thumb, every 20 μm of hull roughness adds 1% to the required propulsion power (Townsin et al. 1980).

Low-surface-energy (LSE) coatings or foul release coatings create non-stick surfaces similar to those known in Teflon-coated pans, but best-practice LSE coatings reach barnacle adhesion strengths 10−20 times lower than Teflon. On the other hand, dynamic tests on moving ships have shown that well-attached barnacles (e.g. after longer stays in port) may require relatively high ship speeds to be released (Swain 2010). Some publications claim fuel savings in excess of 10% due to LSE coatings as compared to copper-based 'standard' coatings. These figures are misleading. Large improvements may be measured directly after coating, with the prerequisite hull cleaning, blasting and possibly also propeller cleaning. However, an appropriate assessment should consider the period between dry dockings. Here, a major supplier of marine coatings gives average savings of 4% for a supertanker, which can be seen as the upper limit for this ship type. All other ship types will have smaller savings, corresponding to the percentage that frictional resistance contributes to total resistance.

Coatings based on nanotechnologies have been on the market for several years and enjoy increasing popularity. It is difficult to judge claims concerning their fuel-saving potential, but a major supplier of marine coatings rated in 2010 their fuel-saving potential not higher than that of LSE coatings.

Surface-treated composites (STC) use embedded glass flakes to achieve a hard outer finish. This hard surface can be cleaned without damaging the coating. In principle, one coating would then suffice for the lifetime of a ship, but in practice local touch-ups may still be necessary. This approach is seen by many experts as very promising.

Air lubrication has attracted considerable media and industry attention. The basic idea is that a layer of air (on part of the hull) reduces the frictional resistance. The considerable technical

effort is most attractive for large, slow ships with small draft. Air lubrication concepts can be classified into (Foeth 2008): air bubble concept (injection of air bubbles along the hull), air cavity concept (recesses underneath the hull are filled with air), and air film concept (using a larger film of air to cover the ship bottom).

There is no consensus on the saving potential with estimates ranging from −5% (i.e. increased fuel consumption) to 15% fuel savings. With no reliable, third-party evaluation, it remains to be seen whether this technology lives up to its claims.

3.7.4. Optimization of Hull and Appendages

Much can be gained in fuel efficiency in the proper selection of main dimensions and ship lines. Ship model basins should be consulted to assess the impact of main dimensions based on their experience and databases. For given main dimensions, wave resistance offers the largest design potential, as moderate changes may yield significant improvements. In most cases fast codes based on simplified potential flow models suffice (Abt and Harries 2007). For fuller hull shapes (tankers, bulkers), viscous flow computations are required, as viscous pressure resistance and hull−propeller interaction are significant. For limited computational resources, simplified approaches using resistance and wake fraction may be used, but proper simulations of the propulsion case at full scale are expected to become standard as computer hardware increases in power. Gains of formal optimization vary between 1.5% and 17%, with 4−5% as typical value.

The term appendages includes here negative appendages, i.e. recesses, e.g. for side thrusters or sea chests. Appendages contribute disproportionately to the resistance of a ship. Hydrodynamic analyses (model tests or CFD simulations) can determine proper local design and alignment of appendages.

Rudders offer an often underestimated potential for fuel savings. Improving the profile or changing to a highly efficient flap rudder allows reducing rudder size, thus weight and resistance. Due to the rotational component of the propeller, conventional straight rudders (at zero degree rudder angle) encounter oblique flow angles to one side at the upper part and to the other side in the lower part. This creates for most rudder profiles a slight additional thrust which recuperates part of the rotational losses of the propeller and improves propulsion. Some experts therefore recommend straight rudders. Others argue in favor of twisted rudders (e.g. Hollenbach and Friesch 2007). Dedicated CFD analyses are recommended to resolve these contradictions and to quantify expected savings in actual projects.

Ships are usually optimized for the trial or design speed in calm water, but later operated most of the time at lower speeds, even when they are not slow steaming. Fuel consumption is expected to be lower if a ship were to be designed for a more realistic mix of operational speeds, load conditions, and environmental conditions. The fuel savings gained are estimated to be 0.5−1.0% at the expense of a higher design effort.

3.7.5. Improved Propeller Designs

Modern CFD methods should lead to better propeller design, especially if design methods progress to reliable prediction of full-scale wake fields and hull−propeller interaction, considering speed and load case ranges instead of just a single operation point. Such improved propeller design procedures may be in place within the next 10 years. Potential savings of 1−4% were estimated by experts from various ship model basins in a confidential survey. The variability of propeller design and the high degree of interaction with the hull make it difficult to predict globally a fuel-saving potential.

Propellers with tip-modified blades form one special class of high-efficiency propellers. These propellers increase the efficiency without increasing diameter, similar to the tip fins often seen on aircraft wings. There are several variations on the theme (ITTC 1999, Carlton 2007):

- contracted and loaded tip (CLT) propellers with blade tips bent sharply towards the rudder (Perez Gomez and Gonzalez-Adalid 1997);
- Sparenberg−DeJong propellers with two-sided shifted end plates (Sparenberg and de Vries 1987);
- Kappel propellers with smoothly curved winglets (Andersen et al. 2002).

In interviews, propeller experts estimated 4−6% efficiency gains feasible for tankers and bulkers, but only negligible savings for ferries. Tip-modified propellers seem best suited for ships trading long-distance at a given speed.

3.7.6. Propulsion-Improving Devices (PIDs)

The propeller transforms the power delivered from the main engine via the shaft into a thrust power to propel the ship. Typically, only two-thirds of the delivered power is converted into thrust power. Various devices to improve propulsion − often by obtaining a more favorable flow in the aftbody − have been developed and installed since the early 1970s, motivated largely by the oil crisis (Blaurock 1990, Östergaard 1996). Some of the systems date back much further, but the oil crisis gave the incentive to research them more systematically and to install them on a larger scale. ITTC (1999) discussed extensively assorted propulsion-improving devices. Opinions on these devices differ widely, from negative effects (increasing fuel consumption) to more than 10% improvements. Model tests for these devices suffer from scaling errors, making any resulting quantification of savings for the full-scale ship questionable. Instead, CFD simulations for the full-scale ship are recommended to evaluate the effectiveness of a propulsion-improving device in design; the detailed insight in CFD simulations also allows a better comprehension of why a device is effective or not. While the absolute prediction accuracy of CFD is still questioned by many experts, the relative gain between two variants (with and without a duct, for example) is predicted with much higher accuracy.

Many devices have been proposed to recover rotational energy losses of the propeller. These can be categorized into pre-swirl (upstream of the propeller) and post-swirl (downstream of the propeller) devices. Devices can only recover losses partially; 30−50% of the losses are an upper limit of what a device may recuperate. Buhaug et al. (2009) give the following indicators for rotational losses:

- tanker/bulker: 3.4% at 10.9 knots, 3.9% at 15.6 knots
- container vessel: 3.9% at 15.5 knots, 5.3% at 21.2 knots
- multi-purpose vessel: 4.5% at 9.5 knots, 6.0% at 13.4 knots
- ro-pax vessel: 4.7% at 14.7 knots, 5.0% at 20.1 knots.

This would indicate (optimistic) upper limits for fuel-saving potential for devices targeted at rotational losses of 1.5−2% for tankers/bulkers, 2−2.5% for container vessels, 2−3% for MPVs and 2−2.5% for ro-pax vessels. Rudders behind the propeller already recover some of the rotational energy, reducing the fuel-saving potential further. Higher estimates found in various publications are then probably based on considering the propeller in open-water condition without rudder.

Pre-swirl devices are generally easier to integrate with the hull structure. Pre-swirl devices include the pre-swirl fin (proposed by SVA Potsdam) and pre-swirl stator blades. Asymmetric aftbodies (Schneekluth and Bertram 1998; Fig. 3.13) are a very robust way to generate swirl, but involve major changes in design. The added costs in ship construction are named frequently as an argument why asymmetric aftbodies are not considered as fuel-saving devices.

The Grim vane wheel (Fig. 3.14; Grim 1980, Schneekluth and Bertram 1998, Carlton 2007) is a freely rotating device installed behind the propeller (on the tail shaft or the rudder horn). The vane wheel is composed of a turbine section inside the propeller slipstream and a propeller section (vane tips) outside the propeller slipstream. The system appears suitable for a wide range of conventional cargo ships, but only few actual installations have been reported. Operators remain hesitant to use this device, as it appears mechanically delicate and involves considerable investment. There are concerns that collisions with wood or ice floes may damage the vane wheel. Improvements of 7−10% are reported (Breslin and Andersen 1994). The higher values are possible for higher propeller loading.

Rudder thrust fins are foils attached at the rudder. Both x-shaped thrust configurations and configurations with only two blades have been proposed. The blades are designed to generate thrust in the rotating propeller slipstream. Full hull forms (tanker, bulker) are expected to benefit more from such fins than slender ships (container vessels, ro-pax vessels). Fuel-saving potential of up to 9% has been claimed (Buhaug et al. 2009). However, no competent third-party proof for such claims is available and interviews with experts in several ship model basins resulted in rather pessimistic average fuel-saving potential estimates of 0.05%. Stator fins are another post-swirl device fixed on the rudder and intended for slender, high-speed ships like car carriers (Hoshino et al. 2004). No explicit claims on their fuel-saving potential have been published.

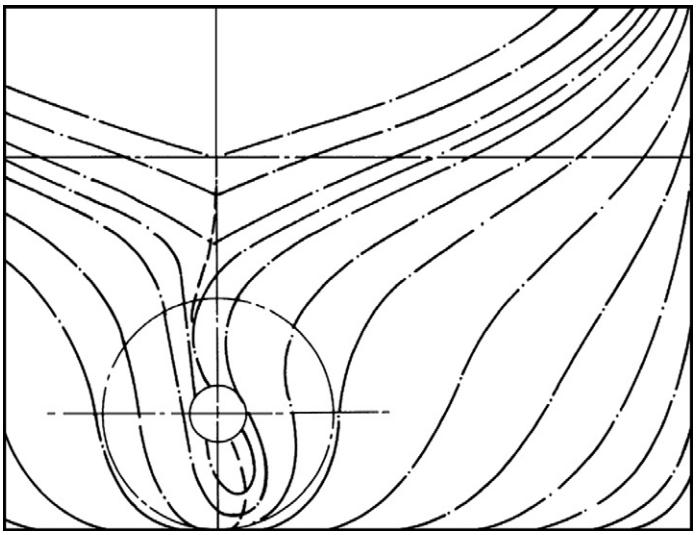

Figure 3.13:
Hull sections of asymmetric aftbody

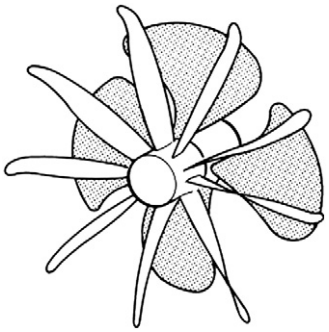

Figure 3.14:
Vane wheel

Contra-rotating propellers combine recuperation of rotational energy losses with better propeller loading (Van Manen and Sentic 1956, Schneekluth and Bertram 1998, Carlton 2007). Reported claims range from 6% to 20% in fuel efficiency improvement. However, contra-rotating propellers also have larger surface, more losses in bearing and recuperate rotational energy that otherwise would be recuperated by the rudder. Buhaug et al. (2009) give much lower estimates of 3−6% based on the estimates of rotational energy losses. This appears to be realistic. The mechanical complexity associated with frequent failure and down-time problems make the adoption of contra-rotating propellers unlikely. However, podded drives and

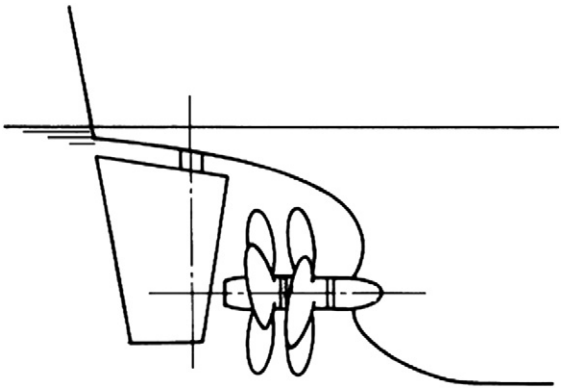

Figure 3.15:
Contra-rotating propeller

conventional propellers have been combined to hybrid CRP–POD propulsion. This option appears attractive for vessels that require redundant propulsion anyway, e.g. dangerous goods tankers.

Devices may be added to the propeller hub to suppress the hub vortex. Propeller boss cap fins (PBCF) were developed in Japan (ITTC 1999). The Hub Vortex Vane (HVV), a small vane propeller fixed to the tip of a cone-shaped boss cap, may have more blades than the propeller. There is no consensus about the effectiveness of the device that is popular due to its low costs, with estimates ranging from 0.1% to 7%.

3.7.7. Wake-Improving Devices

The propeller operates in an inhomogeneous wake behind the ship. The inhomogeneous wake induces pressure fluctuations on the propeller and the ship hull above the propeller, which in turn excite vibrations. The magnitude of these vibrations poses more or less restrictive constraints for the propeller design. A more homogeneous wake then translates into better propeller efficiency. Ideally, the hull lines (including discontinuities like appendages and inlets) should already be optimized in the design stage to have good hull–propeller interaction.

Wake-equalizing devices, such as Schneekluth nozzles, the Sumitomo Integrated Lammeren Duct (SILD) or the Hitachi Zosen nozzle (Carlton 2007), may improve propulsion in suboptimal designs, particularly for full hulls (tanker, bulker). Arguably the best-known wake-equalizing device is the Schneekluth nozzle (Fig. 3.16; Schneekluth 1986, Schneekluth and Bertram 1998). The Schneekluth nozzle is a ring-shaped flow vane with foil-type cross-section fitted to the hull in front of the upper propeller area. The Schneekluth nozzle is the propulsion-improving device with (by far) the most installations.

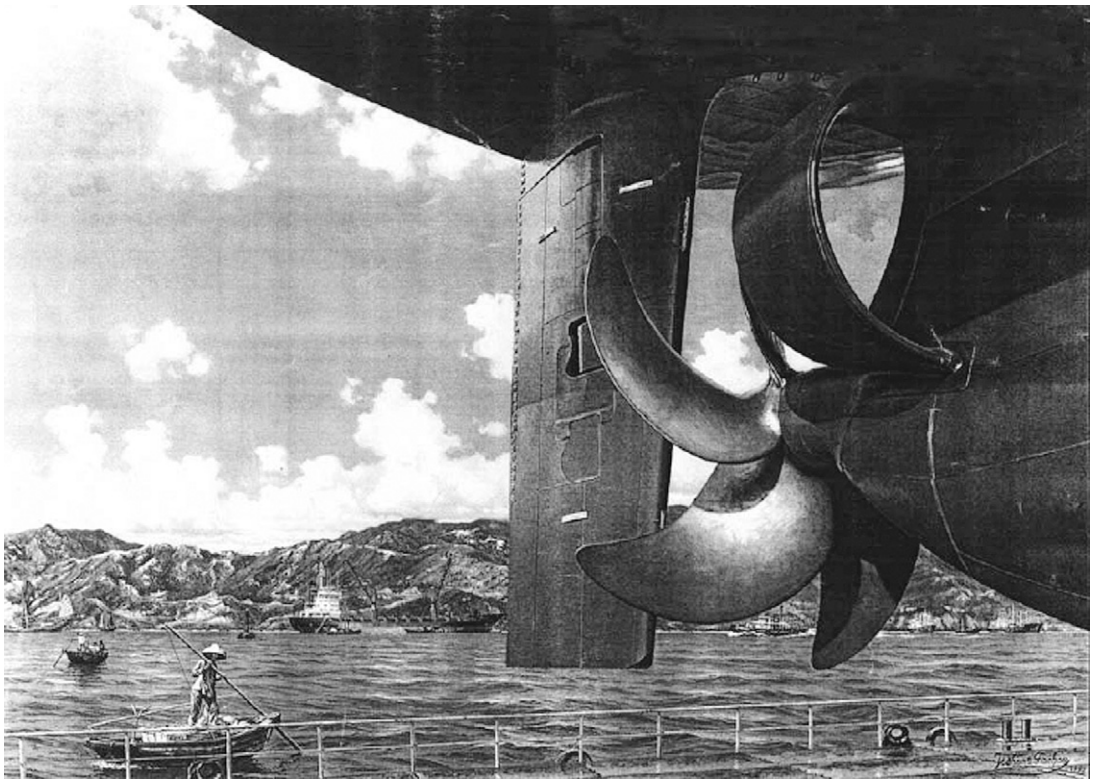

Figure 3.16:
Wake-equalizing duct

Independent analyses came to contradicting evaluations of the effectiveness of wake-equalizing devices (Ok 2005, Celik 2007). ITTC (1999) states cautiously: 'In conclusion, partial ducts may result in energy saving at full scale, but this was not, and probably cannot be proven by model tests.' Mewis (2009) combines a wake-equalizing duct with pre-swirl fins. The same general comments as for wake-equalizing devices apply. The effectiveness may depend on local flow details like the strength and position of the bilge vortex in the propeller plane, making the wake-equalizing devices effective in some cases and ineffective in others. The effectiveness should then be assessed on an individual case base by full-scale CFD simulations.

Grothues-Spork (1988) proposed spoilers – fitted before the propeller on both sides of the stern post – to straighten horizontally the boundary layer flow right before the propeller, thus creating direct thrust and improving the propeller efficiency. He used parts of a cylindrical surface such that they divert stronger near the hull and less further out. These fins are called Grothues spoilers (Fig. 3.17). Older literature, as quoted in Schneekluth and Bertram (1998), and Carlton (2007), gives power savings up to 9%, based on model tests. However, they are expected to increase fuel consumption rather than lead to any fuel

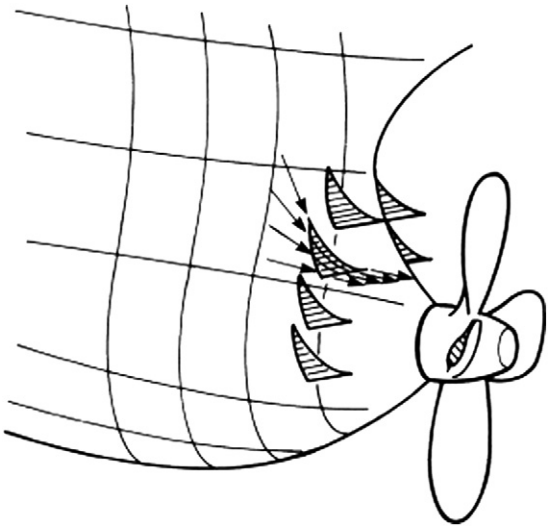

Figure 3.17:
Grothues spoilers

savings. Grothues spoilers and vortex generators have been employed to fix vibration problems in suboptimal designs.

Ducted propellers have been proposed as propulsion-improving devices (Buhaug et al. 2009). Tugs, offshore supply vessels, and fishing vessels frequently feature ducted propellers (Schneekluth and Bertram 1998). The Kort nozzle is an annular forward-extending duct around the propeller (Schneekluth and Bertram 1998). The nozzle ring has a cross-section shaped as a hydrofoil or similar section. The nozzle supplies the propeller with a larger water quantity (increasing ideal efficiency) and the foil shape serves to produce additional thrust. Kort nozzles feature the following advantages and disadvantages:

+ At high thrust-loading coefficients, better efficiency is obtainable. For tugs and pusher boats, efficiency improvements of around 20% are reported. Bollard pull can be raised by more than 30%.
+ The reduction of propeller efficiency in a seaway is lower for nozzle propellers than for non-ducted propellers.
+ Course stability is substantially improved by the nozzle.
− Course-changing ability during astern operation is somewhat impaired.
− Due to circulation in shallow water, the nozzle propeller tends to draw into itself shingle, stones, and ice floes.
− Due to the pressure drop in the nozzle, cavitation occurs earlier.

Only a small number of tankers were fitted with ducted propellers, back in the 1970s. Then ducts were no longer used for large ships, probably due to vibration and cavitation problems.

These problems could be overcome in view of present analysis capabilities (CFD and finite element analyses), leading to a renaissance of ducted propellers for large ships.

3.7.8. Wind-Assisted Ships

Wind was the predominant power source for ships until the late 19th century. Wind assistance has enjoyed a renaissance in recent years. Wind-assisted ships are mainly driven by engine propulsion. Sails are then used to reduce necessary power for a given service speed, provided that the wind is favorable in force and direction. Wind assistance becomes increasingly unattractive with increasing ship speed and decreasing fuel prices. Based on a fuel price of $500 per ton, the systems may be attractive for ship speeds below approximately 14–16 knots. Stability considerations, safety aspects (view field from the bridge) and cargo-handling aspects prevent wide use of sail assistance. For modern cargo vessels, automatic systems are the only viable option and the additional structural effort for mast support on ships with sails can be considerable. Sails for cargo vessels are typically high-performance rigid sails allowing automatic handling and giving propulsive forces even in apparent wind directions in the forward sector. Kites and Flettner rotors are generally more efficient than sails per surface area, but smaller in overall size. Optimum solutions depend on many parameters, most notably ship type, route, and speed.

Modern sails can be controlled automatically. They may be reefable cloth type (sail wings) or rigid profile type such as wing sails.

Kites have been brought to commercial maturity. Kites harness wind power at larger heights without the stability penalties of high masts. They move with much higher speeds than wind speed through the air, exploiting lifting forces similar to foils. By 2010, four ships were equipped with kites, 3 years after the first installation. Kites are claimed to be 25 times as effective (per given surface area) as regular sails. By May 2011, the largest available size was a 32 t pull (320 kN) kite. Kites with up to 130 t pull are envisioned. Savings of 10–35% are claimed for smaller ships on transatlantic routes.

Flettner rotors are another technology harnessing wind energy for ship propulsion. After 80 years of obscurity, they resurfaced in 2010 with the delivery of the E-Ship 1, a freighter equipped with Flettner rotors. These four cylinders, each 27 m tall and 4 m in diameter, are claimed to save 30% of the conventional fuel needed by the ship (10 000 tdw at 17.5 kn design speed, 7000 kW installed power). Flettner rotors create additional wind resistance for head winds and typically increase air draft (unless they are retractable, which requires additional system effort and complexity).

Solar power and wind power can be combined, using fixed sails equipped with solar panels. This option is employed successfully on the SolarSailor ferry operated in Sydney. The fuel-saving potential for large cargo vessels should be comparable to that of best-practice sails.

Sufficiently large units are yet to be developed and the technology, including high-performance solar panels, is still expensive.

There are few wind-assisted modern cargo ships. Kites are most mature with four installations (August 2010). The potential of other wind assistance options may be similar in magnitude. The saving potential differs largely between ship types, ship sizes, and trading routes. Therefore detailed studies are recommended on an individual case basis.

Reported fuel savings for wind assistance are probably in significant part due to reduced ship motions due to the dampening effect of sails. In many wind conditions, the sails cause more resistance and side drift than propulsion and are thus counter-productive.

3.7.9. Voyage Optimization

Trim optimization: for each draft and speed, there is a fuel-optimum trim. For ships with large transom sterns and bulbous bows, the power requirements for the best and worst trim may differ by more than 10%. Systematic model tests or CFD simulations are recommended to assess the best trim and the effect of different trim conditions. Decision support systems for fuel-optimum trim have been proven to result in considerable fuel savings for relatively low investment (Hansen and Freund 2010). For full hulls (tanker, bulker) the saving potential is smaller.

Weather routing (i.e. optimization of a ship's course and speed) may reduce the average added resistance in seaways. Buhaug et al. (2009) give 1−5%. The saving potential beyond what is already widely done may be less than 1% in practice. It depends among other factors on the routes which are traded (for example, Mediterranean or Atlantic).

Even engine load profile (rather than an even speed profile) offers considerable saving potential (Söding 1992). An even load profile during an entire voyage requires accurate ship models and accurate prediction at the beginning of the voyage of weather, currents, and possible other constraints during the voyage.

Adjusting an autopilot to more fuel-efficient setting has been claimed to save up to 2.5% fuel, but no reliable source is known. A significantly lower value appears to be more realistic for most large ships under professional management.